Master Thesis

Analysis and Evaluation of an In-Situ Resource Utilization Based Structure of a Lunar Greenhouse

A thesis presented for the degree of
Master of Science

University of Bremen
Faculty of Production Engineering
Master of Space Engineering I

Yannis Koch 4434423

1. Supervisor: Dr.-Ing. Volker Maiwald
2. Supervisor: Dr.-Ing. Paul Zabel

11 January 2024

Abstract

Future lunar space missions may include the presence of humans on the moon. EDEN NG is a project elaborating a design of a lunar greenhouse which is added to the lunar habitat. It has the capability to provide fresh food and can work as a biogenerative life support system. The thesis analyses and evaluates an in-situ resources utilization based structure of a lunar greenhouse to investigate the mitigation of transport costs. Laser sintering performed best in a trade-off with five other manufacturing methods. The components of the laser sintering method are estimated to have a mass of 2,199 kg.

The primary structure is composed of an inflatable and a sintered regolith shielding. The inflatable is a horizontal cylinder with a length of 6 m and a diameter of 4.2 m. One end is connected to an adapter ring for connection to the habitat and the other end is closed by a half-sphere with a diameter of 4.2 m. It sits in the regolith shielding which has a minimal thickness of 1 m. A FEM analysis showed that the sintered regolith needs to have a tensile strength of minimum 1.05 MPa, a compressive strength of minimum 0.311 MPa and a minimum shear strength of 0.67 MPa which includes a safety factor of 3.0.

The first greenhouse module requires a transport mass of 12,825 kg. Only considering the mass, this approach is cheaper than the EDEN NG approach.

Universität Bremen

Nachname **Koch** Matrikelnr. **4434423**

Vorname/n **Yannis**

A) Eigenständigkeitserklärung

Ich versichere, dass ich die vorliegende Arbeit selbstständig verfasst und keine anderen als die angegebenen Quellen und Hilfsmittel verwendet habe.
Alle Teile meiner Arbeit, die wortwörtlich oder dem Sinn nach anderen Werken entnommen sind, wurden unter Angabe der Quelle kenntlich gemacht. Gleiches gilt auch für Zeichnungen, Skizzen, bildliche Darstellungen sowie für Quellen aus dem Internet.
Die Arbeit wurde in gleicher oder ähnlicher Form noch nicht als Prüfungsleistung eingereicht.
Die elektronische Fassung der Arbeit stimmt mit der gedruckten Version überein.
Mir ist bewusst, dass wahrheitswidrige Angaben als Täuschung behandelt werden.

B) Erklärung zur Veröffentlichung von Bachelor- oder Masterarbeiten

Die Abschlussarbeit wird zwei Jahre nach Studienabschluss dem Archiv der Universität Bremen zur dauerhaften Archivierung angeboten. Archiviert werden:

1) Masterarbeiten mit lokalem oder regionalem Bezug sowie pro Studienfach und Studienjahr 10 % aller Abschlussarbeiten
2) Bachelorarbeiten des jeweils ersten und letzten Bachelorabschlusses pro Studienfach u. Jahr.

☑ Ich bin damit einverstanden, dass meine Abschlussarbeit im Universitätsarchiv für wissenschaftliche Zwecke von Dritten eingesehen werden darf.

☐ Ich bin damit einverstanden, dass meine Abschlussarbeit nach 30 Jahren (gem. §7 Abs. 2 BremArchivG) im Universitätsarchiv für wissenschaftliche Zwecke von Dritten eingesehen werden darf.

☐ Ich bin nicht damit einverstanden, dass meine Abschlussarbeit im Universitätsarchiv für wissenschaftliche Zwecke von Dritten eingesehen werden darf.

C) Einverständniserklärung über die Bereitstellung und Nutzung der Bachelorarbeit / Masterarbeit / Hausarbeit in elektronischer Form zur Überprüfung durch Plagiatssoftware

Eingereichte Arbeiten können mit der Software *Plagscan* auf einen hauseigenen Server auf Übereinstimmung mit externen Quellen und der institutionseigenen Datenbank untersucht werden.
Zum Zweck des Abgleichs mit zukünftig zu überprüfenden Studien- und Prüfungsarbeiten kann die Arbeit dauerhaft in der institutionseigenen Datenbank der Universität Bremen gespeichert werden.

☑ Ich bin damit einverstanden, dass die von mir vorgelegte und verfasste Arbeit zum Zweck der Überprüfung auf Plagiate auf den *Plagscan*-Server der Universität Bremen hochgeladen wird.

☐ Ich bin ebenfalls damit einverstanden, dass die von mir vorgelegte und verfasste Arbeit zum o.g. Zweck auf dem *Plagscan*-Server der Universität Bremen hochgeladen u. dauerhaft auf dem *Plagscan*-Server gespeichert wird.

☐ Ich bin nicht damit einverstanden, dass die von mir vorgelegte u. verfasste Arbeit zum o.g. Zweck auf dem *Plagscan*-Server der Universität Bremen hochgeladen u. dauerhaft gespeichert wird.

Mit meiner Unterschrift versichere ich, dass ich die oben stehenden Erklärungen gelesen und verstanden habe.
Mit meiner Unterschrift bestätige ich die Richtigkeit der oben gemachten Angaben.

11.01.2024

Datum Unterschrift

Contents

List of Tables

List of Figures

List of Abbreviations

Al_2O_3	alumina
BLDC	brushless DC
BLSS	Biogenerative Life Support System
$CaCO_3$	calcium carbonate
CFD	Concurrent Facility Department
FEM	Finite Element Method
FeO	iron oxide
FeS	Troilite
IRMS	Induced Roll Magnetic Separator
ISPR	International Standard Payload rack
ISRU	In Situ Resource Utilisation
KMF	Künstliche Mineralfasern (artificial mineral fibres)
KOH	potassium hydroxide
$MgCl$	magnesium chloride
MgO	magnesium oxide
MLI	Multi Layer Insulation
MMOD	Micrometeorite Orbital Debris
NaOH	caustic soda
PRMS	Permanent Roll Magnetic Separator
OPC	Ordinary Portland Cement
SiO_3	Silicate
TRL	Technical Readiness Level

Chapter 1

Introduction

1.1 Motivation

There have been no astronautical missions going beyond low earth orbit since the Apollo program was terminated [1]. Following the successful Artemis 1 mission, the US-authority NASA is planning to send humans on an orbit around the Moon by the end of 2024 for the first time since 51 years [2] [1]. Private commercial companies such as SpaceX are aiming to bring humans to the Mars by the end of the decade [3]. Although, these goals must be viewed carefully, the development of the Starship, the biggest rocket in the history of space flight, is a fundamental step to bring humanity back to the Moon and beyond [4].

Astronauts will stay for longer periods on the lunar or martian surface and permanently occupied lunar bases are considered [1]. Therefore, proper shelter and infrastructure is mandatory to protect the astronauts against the harsh environment including the vacuum, extreme temperatures, radiation and micrometeorites. Facilities, institutes and companies around the world are currently working on concepts for extraterrestrial habitats [5]. To protect the astronauts from solar radiation and impacts of micrometeorites, it is necessary to get a sufficient amount of mass between the astronauts and the harsh environment [6]. As the transport of mass is still very expensive, ISRU is a pillar of designing extraterrestrial habitats.

One of these lunar habitation projects is the EDEN Next generation (NG) project. The goal is to develope a greenhouse module for a lunar habitat that can provide fresh food produced on-site and can function as a biogenerative life support system (BLSS) [7]. This could reduce the transport of food from the Earth in the long term, provide fresh food which can not be transported for longer missions, and increase the well-being factor of the astronauts [7]. The greenhouse module would function as a cargo module during transport and as a greenhouse module once landed, unpacked and docked to the habitat[7].

The goal of this thesis is to evaluate the usage of on-site resources for manufacturing of a lunar greenhouse to reduce transport costs. For that, five main tasks have been identified. The first one is a review of the state of the art of ISRU concepts for infrastructure manufacturing. With this base, a concept for a regolith based lunar greenhouse module needs to be designed. Additionally, processes for creating the regolith based system and outfitting it with subsystems shall be developed. A CAD model shall be created and analysed. The last task is to perform a cost/benefit analysis of the concept.
The final result shall be an evaluation about the feasibility of such a concept.

1.2 EDEN Next Generation

Eden NG is the follow-up project of the EDEN ISS project launched by Schubert et al. [7]. The goal is to further evolve the lunar greenhouse analogue EDEN, which was operated in the Antarctica, to a system that is close to an actual lunar greenhouse. It is planned that EDEN not only functions as a food supply but also as a bio generative life support system (BLSS). The greenhouse will be transported to the Moon in a logistic-to-green (or cargo-to-green) approach in which the structure of the greenhouse will function as a cargo module during transport. Once landed on the lunar surface it will be transported to the habitat and outfitted. [7]

This thesis focuses mainly on the structure of the module. For more detailed information than presented below please refer to [7].

The primary structure, which includes the outer shell, the interface rings, the radial as well as longitudinal stiffening elements, is based on the ISS Columbus module and has a mass m_{prim} of 7,528.32 kg. [7]
The cylinder has a length of 6.6 m and an outer diameter of 4.2 m and the interface ring is based on the Common Berthing Mechanism. [7]

The secondary structure has a mass of 470.52 kg and includes all internal load-bearing structures. [7]
EDEN consists of a growth and a service area (Figure 1.1). In the service section, International Standard Payload Racks are installed whereas the racks in the growth area are custom made and need to be defined. [7]
Floor and ceiling of the module provide storage and need to be defined. [7]

Figure 1.1: Cross section of the Eden NG design. Left image shows the front view and the right image the side view. [7]

1.3 Proceeding

Figure 1.2 shows an illustration of the proceeding. After an investigation of the state of the art a set of requirements is defined. In Chapter 4, one manufacturing method is defined. For that, six different manufacturing methods are elaborated which includes mass and power estimations. A trade-off is performed to define the final manufacturing method.
In Chapter 5, the greenhouse module is designed. The Chapter is divided into the design of the primary and the secondary structure. The primary structure includes an inflatable, and the regolith structure which is analysed with a FEM, In the mission chapter, the results of the prior two chapters are used to define and describe the complete process and includes the cost-benefit analysis.
An overarching discussion (see Chapter 7) focuses on the proceeding and justifies the results against the defined requirements.

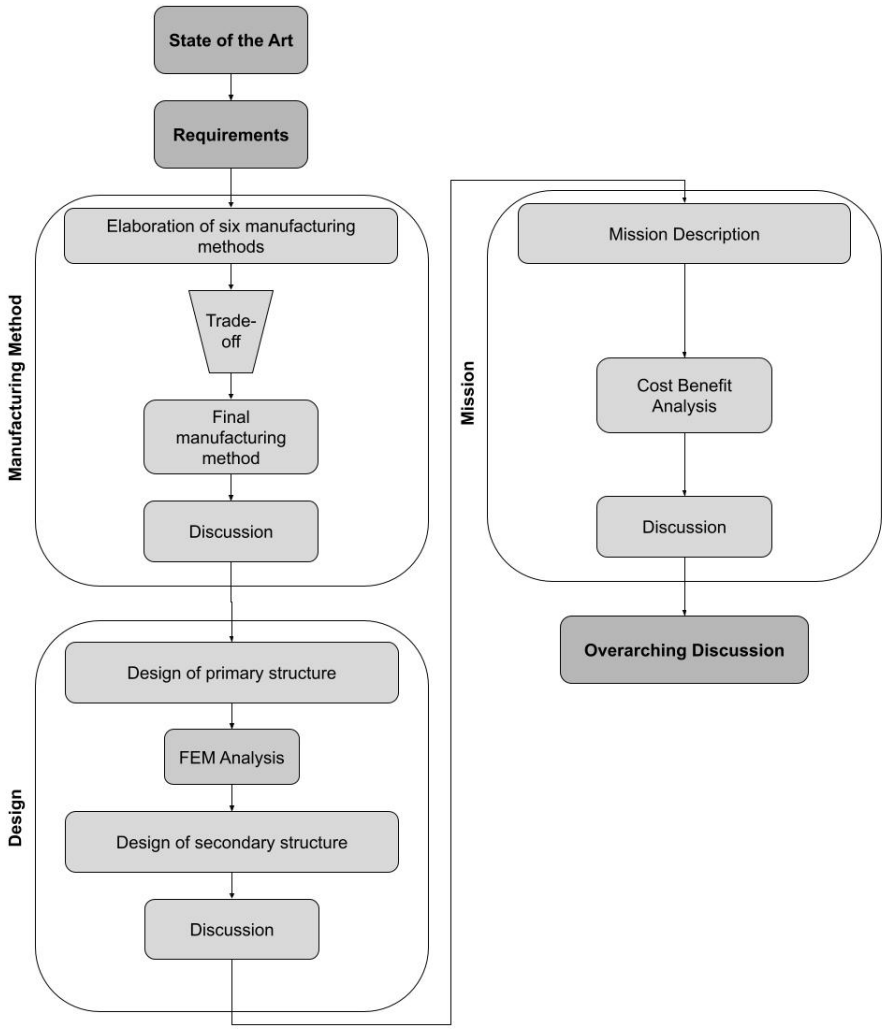

Figure 1.2: Based on the state of the art and the defined requirements six manufacturing methods are elaborated to find the most suitable one in a trade-off. The primary and secondary structure are designed afterwards. The design of the primary structure includes a FEM analysis. All results are used to define and describe the final mission including the cost-benefit analysis. An overarching discussion reviews the overall results.

Chapter 2

State of the Art

This chapter gives information which are required for the design of the manufacturing methods and the greenhouse module. It includes information about the Moon Village, lunar regolith, processing technologies and manufacturing methods.

2.1 Moon Village

The Moon Village is an open concept multi partner permanent human settlement on the lunar surface initiated by the ESA Moon Village Initiative [8]. For a concept study of the Moon Village, ESA set a couple of parameters, requirements and assumptions as described in the following. For more details please refer to the CFD study of the ESA Moon Village Initiative [8].

1. The crew size shall be 4 and replaced every 500 days
2. The lifetime after deployment shall be 10 years
3. The module shall provide sufficient radiation protection ($<$ 250 mSv)
4. The concept shall be compatible with state of the art launcher technology
5. It can be assumed that the crew will be on-site to support deployement and construction
6. The habitat will be located at the southpole near the Shackelton crater rim
7. An annual resupply can be assumed
8. The cargo lander will have a payload capacity of minimum 1700 kg
9. Rovers, robotic, tugs and a mobile crane will be available
10. ISRU capabilities were demonstrated and implemented in prior missions

2.2 Lunar Regolith

This chapter will give focused insights on the properties of lunar regolith relevant for the thesis. For a more detailed view, please refer to the Lunar Sourcebook [9].

2.2.1 Physical Properties

Heiken et al. [9] state that the physical properties of lunar regolith are relative uniform over the lunar surface (see Table 2.1). Lunar regolith describes the loose layer of fragmental and unconsolidated rock material of the lunar surface. It is a cohesive, sharp-edged and fine grained material that comes in different shades of grey depending on the composition. Table 2.1 shows the grain size distribution of three regolith samples which were brought by the Apollo missions. Sample 71 061.1 was collected at the mare surface, 72 441.7 at the base of the South Massif, on the "light mantle" deposit and 15 601.96 at the edge of a lava rille. On average, 49.67 wt.% of the lunar regolith has a particle size of less than 75 µm and all samples have the biggest fraction ($>$ 17 wt.%) in the $<$ 20 µm section. [9]

2.2.2 Chemical Composition

In opposite to the mechanical properties, the chemical composition varies significantly over the lunar surface. Haskin and Warren categorize the lunar material into mare basalts, highland monomict rocks and soils and regolith breccias. They define the soil category as the $<$ 1 cm fraction of loose lunar surface debris. Oxygen (O) is the major element of the lunar material. The atoms are tightly bound to other elements and make up 45 wt.% followed by Silicon (Si) with 21 wt.%. Aluminum (Al) contents vary between 5 wt.% for the mare basalts and 13 wt.% for the highland samples. 15 wt.% of the mare basalt samples are iron

Table 2.1: Grain size distribution of three different samples. Sample 71 061.1 *was collected at the mare surface,* 72 441.7 *at the base of the South Massif, on the "light mantle" deposit and* 15 601.96 *at the edge of a lava rille. The fraction of a particle size less than* 20 µm *was not provided for sample* 15 601.96. *[9]*

Particle size [µm]	Fraction [wt.%]			
	71 061.1	72 441.7	15 601.96	Average
250 - 500	7.08	8.55	11.91	9.18
150 - 250	7.04	8.37	13.13	9.51
90 - 150	8.66	11.02	15.99	11.89
75 - 90	3	4.01	5.48	4.16
45 - 75	8.39	12	14.45	11.61
20 - 45	12.21	18.79	17.37	16.12
$<$ 20	17.98	25.84	N/A	21.91

whereas the highland samples only contain 6 wt.%. Magnesium (Mg) makes up roughly 5.5 wt.%. Sulfur (S) can be found in form of sulfide minerals in a fair amount compared to terrestrial basalts ($< 0.08\%$ in ocean-floor basalts). The most common sulfide mineral is Troilite (FeS). The total content of Sulfur varies between highland monomict rocks, mare basalts and soils and regolith breccias. The content of the mare basalts varies between 0.02 wt.% and 0.3 wt.%, for the highland monomict rocks it is less than 0.1 wt.% and in the soils and regolith breccias the content varies between 0.02 wt.% and 0.22 wt.%. [9]

2.2.3 Lunar Regolith Simulant

As not enough lunar regolith was brought to Earth during the Apollo missions to allow all the material intensive research projects, simulants are used to imitate the lunar regolith. There are simulants to imitate the highland or the mare samples and they vary in the chemical and physical properties [10]. However, there is no simulant on the market imitating lunar regolith perfectly [10].
The most common is the JSC-1A simulant from NASA. It has a similar particle size distribution, mineralogy and bulk chemistry as the lunar mare soil samples [11].

2.3 Lunar Regolith ISRU Techniques

2.3.1 Lunar Regolith Excavation

Collecting enough regolith for construction is the first important step for ISRU construction. Just et al. [12] define the drawbar force or also called the excavation force as a very important parameter of an excavation system. It describes the force that the system can utilize to lift material upwards. On Earth, excavation machines are designed very heavy to increase the excavation force. Due to high transportation costs and limitations and the lower gravity, lunar excavation systems must be designed to work with a low excavation force. [12]

Just et al. [12] investigated 13 different lunar excavation projects for a parametric review. They are classified into discrete and continuous systems which are separated into partial and complete systems (see Figure 2.1). Discrete systems need to stop the excavation to either dump the excavated material or to clear the excavation surface. Complete systems include a mobility platform. [12] The excavation capability of the systems investigated by Just et al. [12] varies between 6 - 2400 $\mathrm{kg\,h^{-1}}$ and the mass varies between 67 - 312 kg. They state that continuous systems seem to be more promising as the shallow cuts reduce the required excavation force per cut which leads to a reduced mass. Further, avoiding accumulation of regolith in front of static excavation blades further reduces the excavation forces. Examples are scrapers and dozers. The number of moving parts should be kept low due to the lunar dust and surface environment. Therefore, they prefer bucket drums over bucket wheels as no

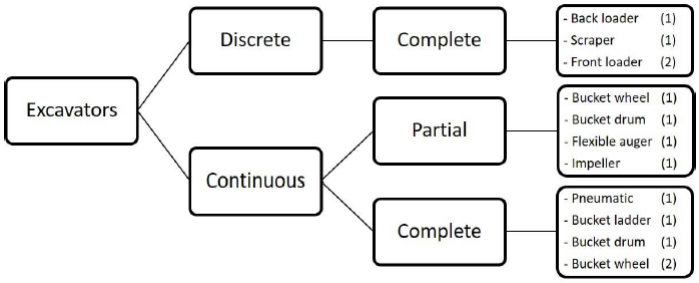

Figure 2.1: The classification of the excavations system from Just et al. [12]. They are separated into discrete and continuous and are further separated into partial and complete systems. Discrete systems need to stop the excavation to either dumb the excavated material or to clear the excavation surface. Complete systems include a mobility platform. [12]

additional transport system is needed. This and the high excavation efficiency makes pneumatic systems promising. However, compressed gas is needed as a consumable. [12]

With a current TRL of 4 the Regolith Advanced Surface System Operation Robot (RASSOR) is a promising bucket drum system [13]. In their final report of RASSOR 2.0, Mueller et al. [13] present that the proof-of-concept prototype successfully demonstrated the functionality in a laboratory environment (Figure 2.2). They state that the RASSOR 2.0 can excavate a minimum of 112.5 $\mathrm{kg\,h^{-1}}$ with a total mass of 66 kg. The rover excavates the regolith by using two bucket drums while slowly driving forward. Due to the opposite forces of the bucket drums a net zero horizontal force allows a low vehicle traction. The drums can be utilized for climbing slopes. Once the torque sensors indicate that the drums are full, the RASSOR 2.0 needs to deposit the collected regolith in a hopper or storage. [13]

Another interesting approach is the Lunar Excavation and Size Separation System (LES) for the LUVMI-X rover platform, which was designed by Just et al. [15] and includes a sieve for size separation during excavation (Figure 2.3). The LUVMI-X rover weighs between 40 and 60 kg and the LES has a mass of 2 kg. The regolith is excavated with the moving inlet system, sieved and transported after the disposal of the coarse material. In one shove of the inlet arm, 100 g of sieved regolith can be excavated. They showed in a labaratory experiment of the arm, that it is possible to combine excavation and sieving. [15]

Figure 2.2: The Rassor 2.0 was tested in an analogue test bed. The bucket drums collect the sand of the test bed by rotating in opposite direction. [14]

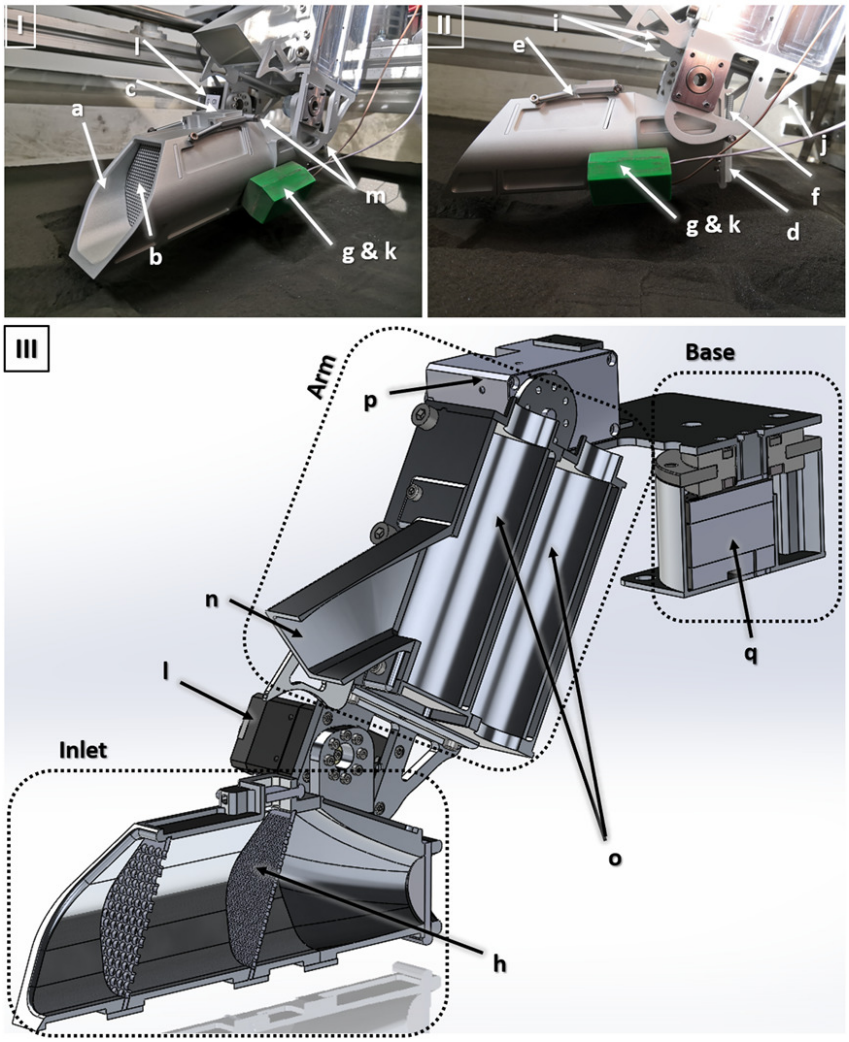

Figure 2.3: Excavation arm of the LES consisting of the inlet including two sieving screens, the arm and the base. The sieving includes a vibration motor. Image from Just et al. [15] : "Features I and II show the inlet with all its components in a laboratory environment and feature III presents a sliced 3D rendering of the whole mechanism with an indication of the three main parts. Individual components are: (a) cylindrical inlet, (b) coarse mesh/sieving plate, (c) outlet for coarse fraction, (d) outlet for fine fraction, (e and f) spring loaded gates, (g) vibration motor, (h) fine mesh/sieving plate, (i and j) cam profiles, (k) vibration motor containment, (l) high-torque stepper motor for inlet actuation, (m) roller bearings, (n) chute for coarse fraction, (o) channels/slides for two size fractions, (p and q) high-torque stepper motors for arm and base actuation."[15]

2.3.2 Regolith Processing

Excavated and collected regolith would potentially need to be processed to achieve either a desired size distribution or chemical composition to allow certain processes or for sufficient properties to be a resource for the contruction process.

Milling

Larger parts of the regolith could be milled until the desired size distribution is reached. However, there is only little research of milling lunar regolith, especially of milling on the lunar surface.

Size Separation

The more common method to achieve a desired particle size in the feed stock is to separate it by size. This can be either done during (see Chapter 2.3.1) or after excavation.
Rasera et al. [16] classify the separation techniques into gravity, electrostatic and magnetic separation. Gravity separation is based on the mass, density and volume differences of the particles. The final maximum particle size can be controlled with the mesh size of the screens. [16] To prevent clogging in the system, vibrational motions can be used [15]. Rasera et al. [16] state that for electrostatic separation the Coulomb and or dielectrophoresis forces are used. The separation happens due to the surface charge of the particles. However, intense classification of the feed stock is mandatory as large particles of one material may have the same charge as small particles of another material. Magnetic separation uses the different susceptibilities of minerals when exposed to a magnetic field for separation. However, there is currently no technology for magnetic size separation. [16]

Adachi et al. [17] developed and tested a electrostatic size separation. The system is composed of a power supply, a particle conveyer which consists of parallel copper electrodes printed on a polyimide substrate and a collection box (Figure 2.4). A voltage in the electrodes forms a electrostatic travelling wave which the particles follow. Due to the gravitational force, too large particles pass underneath the collection box. The System was tested under vacuum conditions with the regolith simulant FSJ-1. The test showed that the system separates small particles (< 20 µm) effectively from the bulk feed stock. [17]

Benefication

Benefication describes the process of removing certain components of a material to increase the fraction of a desired component.
Especially for ISRU it is often mandatory as specific chemical compositions are required, e.g a specific content of sulfur (see 2.3.4) or highly enriched in metal to allow specific processes [16].

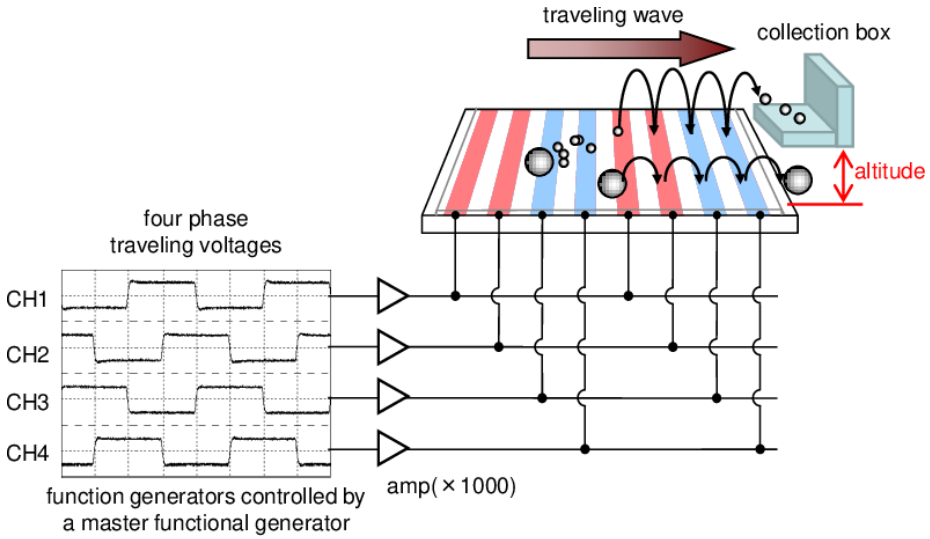

Figure 2.4: Schematic overview of the electrostatic size separation system. The regolith particles are charged on a conveyor plate. Particles which are small enough jump into the collection box, while too large particles fall below the box. [17]

This can be achieved by either separating the desired mineral from the bulk and further process it or by separating unwanted minerals from the bulk until the necessary concentration is reached [16].
As stated in Chapter 2.3.2 there are gravitational, electrostatic and magnetic separation which make use of differences in the respective properties of the particles [16].

Magnetic benefication can be achieved with magnetic roll separators. They are mainly composed of a rotating outside roll and a magnetic inner roll [18]. It is designed such that the magnetic field of the inner roll converges on the roll surface so that feed stock that is loaded onto the roll has a different trajectory depending on the magnetic properties of the particle [18]. Non-magnetic particles are not influenced by the magnetic field and their trajectory is hence not impacted [18]. Magnetic particles have a trajectory changed by the interaction with the magnetic field [18]. It is possible to design systems with multiple levels which differentiate, usually from low to high, in magnetic strength for more accurate separation [19].
According to Christiansen et al. [18] they can be divided into induced roll magnetic separator (IRMS) and permanent roll magnetic separator (PRMS) depending if a electro- or permanent magnet is creating the magnetic field. PRMS require only 10% of the energy, 10-20% of the mass and 60% of the volume compared to IRMS. However, IRMS provide higher flexibility due to the

possibility to change the magnetic field strength. [18]

Metal Extraction

Metals such as aluminum, iron or titanium found on the Moon are usually bound with oxygen in metal oxides [9]. Therefore, it is possible to extract the metals by reduction of the metal oxides [16].

Gonzalez designed a process to extract metal and oxygen from ilmenite via chemical reduction with hydrogen or methane. The ilmenite enriched feed stock is heated inside a reactor before injecting the hydrogen to start the reduction reaction. Once the reduction is finished and material is cooled, the iron (Fe) and titanium dioxide (TiO_2) are just physically bound together and need to be separated. The water formed during the reaction can be further used for electrolysis to form oxygen and hydrogen which can be reused again for reduction. [20]

Sulfur Extraction

The occurrence of Sulfur on the lunar surface is described in Chapter 2.2.2.
Gibson and More showed in a heating experiment that the sulfur which is bound in Troilite (FeS) can be extracted by heating the lunar soil. The extractable sulfur fraction is temperature dependant. By heating the soil between 750 and 1,100 °C, 12 - 95% of the sulfur in the soil can be extracted. The heated sulfur is then given as SO_2 and H_2S. [21]

To process both gases to pure sulfur, a Claus sulphur recovery unit can be used. This unit is based on the Claus process (see Eq. 2.1) in which the SO_2 and H_2S react to sulfur and water. The x can vary between 2 and 8.

$$SO_2 + 2H_2S \rightarrow 2H_2O + \frac{3}{8}S_8 \text{ [22]} \tag{2.1}$$

The Claus process is a mature process and used on Earth to produce sulphur and or treat waste gas [23].
According to Ibrahim et al. [22], terrestrial reactors are composed of a thermal and a catalytic unit. In the thermal unit H_2S is heated to form H_2S and SO_2. Both gases are then let into the catalytic unit. A catalytic unit of a sulfur recovery unit is composed of a pre-heater, catalytic reactor, which uses activated aluminum or titanium oxide as a catalyst, and condenser . The pre-heated gas reacts after contact with the catalysts as described in Eq. 2.1. In the condenser the trace gases are then cooled to extract the sulfur. [22]

Water Extraction

There is clear evidence that water is present on the Moon and especially the polar regions inhibit a significant amount of water ice [24].

Kiewiet et al. [25] performed a trade-off and optimization for thermal water extraction at the lunar poles. They differentiate between in-situ extraction and excavated extraction. For in-situ extraction the icy regolith is heated and the sublimating water vapor is collected via a dome whereas for the excavated extraction, the regolith is excavated and heated in a sealed chamber. They found via simulations that the excavated process provides higher yield rates (Factor 10) and a better efficiency. However, the in-situ processes are significantly simpler, more reliable and have a higher expected lifetime, even though it is not clear, if the higher lifetime can counteract the significantly lower yield rates. All designs have a TRL of 3. [25]

2.3.3 Additive Manufacturing Technologies

Additive Manufacturing describes the process of creating a three dimensional object usually by material deposition [26]. The material, which can vary for different applications, is deposited in layers [26].
Especially in the context of extraterrestrial habitation, additive manufacturing gained attraction as it provides the possibility to use materials on site for construction of heavy infrastructure such as radiation and micrometeorite shielding and therefore reduces transport costs [26].
For the construction of the greenhouse three additive manufacturing technologies, which are based on different binding principles, will be investigated and evaluated in more detail.
Contour Crafting uses, similar to most terrestrial construction, concrete like feed stock [27]. D-Shape on the other side uses a salt (e.g. magnesium chloride) and metal oxide to react as an inorganic binder [6] and the third is mobile sintering where the layered soil is heated to the melting point to form a solid material [26].

Contour Crafting

Contour crafting is an additive manufacturing technology based on the extrusion of concrete in layers through a computer guided nozzle while the outer surface is smoothed out by trowels and combines the extrusion for the outer wall and a filling process of the core [27]. Laboratory experiments have been carried out which results in a TRL of 4. [28].

Figure 2.5 shows the nozzle of a contour crafting extruder. The outer surfaces are smoothed out by the trowels. The inner core can be completely filled, partly filled or filled with a different material such as loose regolith.

In the final reports of phase I and II Khosnevis et al. [30] are presenting the concept to use contour crafting as the construction technology for lunar infrastructure. The idea is to combine a rover, such as the 'ATHLETE' rover, and a 6-axis robotic extruder (Figure 2.6). The total estimated mass of the system

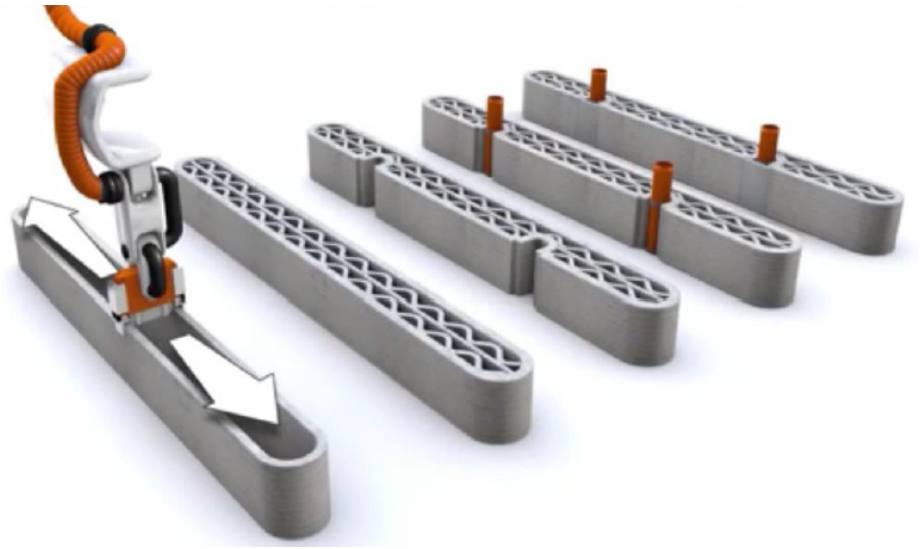

Figure 2.5: Schematic of wall construction with contour crafting. The printing nozzle first prints and smooths out the outer wall before filling the core. Different core designs or inserts are possible. [29]

is 500 kg and has an extrusion rate of 5 $\mathrm{kg\,min^{-1}}$ and an expected power consumption of 3 kW. [30]

Benefits of contour crafting are a higher fabrication speed, the ability to produce large layer heights without compromising the unprecedented surface quality, a wide choice of materials while producing less waste material and increasing the range of designs [27] [28].

There are currently no specific requirements for the size distribution of the feed stock [15].

D-Shape

D-Shape is a patented construction technology. Fine material is layered and the computer designed structure is achieved by adding an inorganic binder and by layering the three dimensional structure can be obtained. [31] [6]

Cesaretti et al. [31] build two demonstrators of D-Shape printers. They are mainly composed of a gantry frame, a spraying head and a printer head. The spraying head injects the ink, so the inorganic binder, on to the layered material, which is straftified by the printing head. The ink is a liquid water / magnesium chloride solution and the layered material is a mixture of the re-

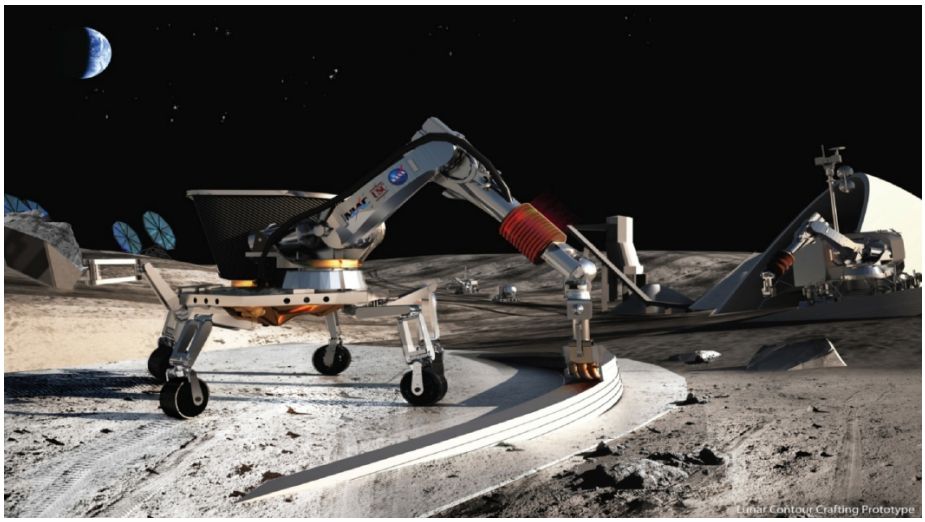

Figure 2.6: Concept of a contour crafting rover. The contour crafting arm is mounted onto an ATHLETE rover. [30]

golith simulant DNA-1 with 25 wt.% of magnesium oxide which reacts with the ink to sorel cement and an artificial double magnesium-carbonate sandstone is created. They also investigated the functionality of the process in vacuum as the ink is a water solution. They come to the result that by directly injecting the ink into the layer, the surface tension of the droplets is sufficient for proper printing and the temperature range is between -10 °C and 60 °C. However, large scale testing is necessary. The created sand stones are very porous and have a compressive strength of 20.35 MPa. The water and the magnesium oxide are resources available on site (see Chapter 2.2.2 and 2.3.2) but magnesium chloride must be transported. Cesaretti et al. [31] designed a dome shaped shelter of 250,000 kg holding an interior volume of 40 m^3 for which 3,800 kg of the dry salt are required. The design proposed by the reseachers is based on an inflatable which is estimated with a mass of 1,000 kg - 1,500 kg. They estimated a total necessary payload mass of 8,000 kg. One major open research point is to allow mobility of the printing system, for example by using robotics and rovers. [31]

Sintering

Sintering is a process to form a solid material from loose feed stock by heating it just under the melting temperature. It is either possible to sinter regolith into blocks (see Chapter 2.4.1) or directly sinter layered regolith [26]. For the direct sintering process, an energy beam such as a concentrated light (see Chapter 2.3.3), microwave or laser beam can be used to heat the regolith [26][32].

Farries et al. [32] investigated the usage of a CO_2 laser as it provides a higher efficiency and deeper penetration depth. The goal is to sinter or melt regolith on the ground to mitigate dust raise and contamination. Therefore, a sintering unit with sufficient power supply will be mounted on a rover and form a solid surface with a laser array. In multiple trials they investigated the parameter of laser sintering and found that a 40 W laser is sufficient to sinter the regolith. This leads to an estimated required power of roughly 700 W for the system. Depending on the input energy a penetration depth of 4 mm can be achieved. The required temperature depends on the regolith simulant and goes up to 1,300 °C. [32]

Solar Sintering

Solar sintering is a special sintering process that directly uses concentrated solar light to sinter the feed stock [26]. As the energy beam is concentrated solar light, external power for the energy beam is not necessary which reduces the power consumption.

In a set of experiments, Meurisse et al. [26] investigated solar sintering. They used a Xenon lamp as a sun simulator to achieve a constant illumination and printed brick shape party layer by layer. The created probes had a compressive strength of less than 5 MPa and showed high levels of porosity and a weak layer to layer bonding. Possible improvements that need investigation are smaller temperature gradients and adapted cooling times [26].

Urbina et al. [33] are working on lunar solar sintering systems within the Regolight project. They designed a mobile printing head with a TRL of 4. For sun light concentration a 2 kg fresno lense is used. The design includes a feed stock feeding system and a carriage. This mobile printing system could be mounted on a rover such as the ATHLETE rover. [33]

2.3.4 Lunar Concrete

Concrete is a fundamental material for terrestrial construction and could play this role on the Moon as well. Especially the contour crafting technology is based on lunar concrete [27].
Concrete consists of granular aggregates that are connected by a matrix of a binding mix [34]. There are different possibilities for the binding mix.

Hydraulic Concrete

Ordinary concrete uses water that is mixed with dry portland cement to bind the aggregate material by starting hydration reactions which continue until fully reacted while excess water evaporates [34].

The occurrence of water ice and the extraction possibilities are described in

Chapter 2.3.2.

Ordinary Portland Cement (OPC) production is a complex process. Habert et al. [35] describe OPC as a four component system of CaO, SiO_2, Al_2O_3 and Fe_2O_3. Limestone, silicon, aluminum and iron ore is first crushed and blended. This raw meal is heated up to 1,500 °C at which calcium silicates and aluminates are formed. After cooling, the produced clinker is milled again with gypsium and other additives to produce cement. [35]
No research on lunar cement production has been found.

Aggregates would be processed lunar soil [30]. The excavated lunar soil (see Chapter 2.3.1) would need to be separated by size according to the downstream requirement of the manufacturing technique.

Cullingford et al. [34] tested the concrete hardening process under vacuum conditions and state that test object which was hardened under vacuum conditions provides similar compressive strength as the control which was hardened under ambient conditions. In vacuum the excess water evaporated faster without any cement dehydration. [34]

Sulfur Concrete

Although available on the Moon, water is not only a very valuable resource, but also complicated to handle when not present in a solid state under vacuum conditions. Additionally, curing of portland or other hydraulic cement takes up to 28 days under terrestrial conditions [36]. Finding an option without the need of water is desired.

One possible candidate as a substitute would be sulfur which could potentially replace the cement and water binding mix [37]. By heating a sulfur/regolith mixture over the sulfur melting point of 120 °C, for example by extruding it through a heated nozzle of a contour crafting system, a concrete like structure is created [30]. This also leads to the objective that the structure should not be exposed to temperatures above 120 °C. The temperature at the lunar southpole varies between -249.8 °C and 65.92 °C [38].

Sulfur can be obtained on-site (see Chapter 2.3.2).

Toutanji et al. [37] tested sulfur concrete with varying sulfur contents and the JSC-1 lunar simulant. The sulfur content varies between 12 and 22 wt.%. The sulfur concrete samples provide a higher compressive strength than hydraulic concrete with a compressive strength of 31 MPa. [37]
Khoshnevis et al. performed first tests of sulfur concrete extruded via contour crafting. Instead of JSC-1 simulant they used washed dry sand with similar size distribution as the JSC-1 simulant and a maximum particle size of less than 1 mm as the chemical composition is not influencing the binding strength of

the sulfur concrete. Different to Toutanji et al. ([37]) the sulfur content varied between 30 and 40 wt.% with a defined optimum at 35 wt.%. Any mixture below a sulfur content of 30 wt.% let to fast blocking due to very high friction and mixtures above 40 wt.% were too liquid for proper extrusion. The extruded concrete probes had an average compressive strength of 3.65 MPa and a maximum at 7.79 MPa. Khoshnevis et al. [30] expect that a higher pressure during the extrusion process will compact the concrete more and therefore reach higher compressive strengths. They also found that sulfur concrete is very fast curring and reaches 90% of its final strength after 6 h and is sufficiently hardened after 2 min for layering. Additionally, it is completely recyclable and has a strong interlayer binding. As extrusion of an abrasive material like the dry sulfur regolith mixture is rather complex, they made extensive research on the extruder system. The low gravity, vacuum, temperature varations and dust effects have been considered. A vibration unit was included to overcome clogging caused by the dry mixture and the "bridging phenomenon". The "bridging phenomenon" describes the phenomenon that in a flow of dry particles few particles create an arch against the nominal flow which causes a pushing against the inner walls and therefore leads to clogging. [30]

To limit radiation exposure to 800 mSv a wall of sulfur concrete (35 wt.% sulfur) with a thickness of 6.7 cm would be sufficient [37]. Toutanji et al. [37] showed that the radiation shielding can be significantly improved by adding 1 wt.% of Polyethylene as the shielding thickness of lunar regolith is reduced from 6.9 cm to 3.81 cm [37].

Due to the very low pressure, sublimation effects of the production material need to be considered [39].
Grugel et al. [39] investigated and tested the sublimation effect of sulfur at vacuum conditions. They tested pure sulfur and two sulfur concrete samples in a vacuum chamber (5×10^{-7} torr) at room temperature (18 - 21 °C) over 60 days. The samples showed sublimation effects and the researchers estimated with the results and mathematical models that at 20 °C a 1 cm thick sulfur wall would sublimate away after roughly 955 days. [39]

Geopolymer Concrete

Another option to bind the loose regolith is geopolymer concrete. Lee and Riessen reviewed the potential usage of geopolymer more precisely an amorphous aluminasilicate inorganic binder to replace ordinary portland cement for lunar construction. It is produced by mixing an alkali activator with a proper amorphous aluminasilicate source material such as metakaolin or coal-fired fly ash. They name regolith as a promising source for amorphous aluminiasilicate as it is estimated to contain 42 wt.% - 47 wt.% SiO_2 and 15 wt.% - 17 wt.% Al_2O_3. For mixing of the geopolymer, water addition is necessary. However, as after hardening only 0.8 - 1.77% residual moisture were measured in the final sample, evaporating water could be potentially recycled by sealing the curing

process. This is also necessary to keep the moisture inside during the mixing process. Most commonly caustic soda ($NaOH$) or potassium hydroxide (KOH) are used as a liquid alkali activator in a two-part geopolymer mixture. $NaOH$ has a high viscosity which reduces at lower temperatures. So careful selection of mixing and curing times is mandatory. KOH has a lower viscosity but a more exothermic reaction when mixed with water. Another option is to create a one-part geopolymer by adding free water to a mixture of a dry alkali acticator and the amorphous aluminiasilicate. Potential dry alkali activators are solid sodium silicate, caustic soda powder, calcium oxide or magnesium oxide. When cured at ambient temperatures in air, geopolymer concrete has a sufficient compressive strength for lunar construction when assumed that 6 MPa as a sufficient compressive strength. Curing in a vacuum environment reduces the ultimate compressive strength by 50% and increases the porosity. However, when the temperature is simultaneously increased to 30.7 - 99.6 °C the compressive strength can be increased. Additionally it is reported that the compressive strength increases also when the geopolymer is exposed to large temperature cycles (-80 - 114 °C; -190 - 25 °C). A careful selected mixing and curing scheme is mandatory [36].

Reinforcement

Glass fibres are a common additive to reinforce, so increasing certain properties as tensile strength, materials [40]. As a large fraction of the lunar soil has a glass phase [9], glass fibre reinforcement is an option to improve the properties of lunar regolith structures [40].

Toutanji et al. [40] showed that adding glass fiber to lunar concrete (sulfur/JSC-1A simulant) can increase the strength by 45%. They manufactured the glass fibres by heating JSC-1 between 1450 °C and 1600 °C and hand drawing them with a aluminum rod through pads soaked in a polyamide solution. The fibres are then cured for 12 h at 200 °C to obtain a polymer coating. [40]

Especially the low tensile strength of lunar concrete can be increased by fiber reinforcement [23]. Khoshnevis et al. [23] found that adding metal powder of up to 5 wt.% also increases the tensile strength [23].

2.3.5 Pressurizability

The manufactured structure must ensure very low air leakage to allow a constant pressure inside the module without continuously pumping gas inside the module. One option is to manufacture the regolith structure in such way that it is completely air tight and the other one is to use an inflatable which is covered by the regolith structure and keeps the pressure of the module.

Inflatables

Inflatables are most times flexible, foldable structures, they are typically lightweight, and provide a very good ratio of transport to final volume [41].

They are composed of a bladder, a restraint and a thermal and micrometeorite protection layer [41]. Cadogan et al. [41] state that the bladder is a polymer coated fabric or durable film to contain the gas and therefore the pressure inside the volume whereas the restraint is a textile or webbing and reacts the inflation and dynamic system loads. The thermal and micrometeorite protection layer includes multiple layers of aluminized Mylar for thermal protection, spacer and a hypervelocity protection material such as Kevlar. [41]

Biesbroek et al. [8] differentiate the inner and outer section of the inflatable. The main purpose of the inner layer is to contain the air inside the module. It is composed of a liner which is usually made of a durable and flame resistant meta aramid, a bladder separation layer made out of aramid/Kevlar and the air containment bladder which is made out of a low permeability material such as CEPAC HD200. The outer layer is composed of the restraint layer which takes up the outward working force caused by the inner pressure, micrometeoroid orbital debris (MMOD) insulation, multi layer insulation (MLI) and an optional external protection layer. Driving evaluation criteria for inflatables, especially the air containment layers, are flammability, rigid/inflatable interface, flexibility at low temperatures, puncture resistance, leakage rate and packing efficiency. [8]

There is room for further development of the material as Cadogan et al. [41] show with their research on Intelligent Flexible Materials for Deployable Space Structures (InFlex). They are working on several improvement such as embedded health monitoring, self healing material and are including anti-microbical protection and radiation shielding. A test of a 0.75 m x 0.75 m assembly showed positive results of the health monitoring and the passive self healing of penetrations < 2 mm after ballistic and puncture testing. [41]

As gas will always escape through tiny imperfections of the material, rigidization of the inflatable is option which can be achieved via the characteristics of the resin (UV-setting, thermosetting, glass transition) or stretched metal laminates [8]. For further infomation, please refer to the ESA CFD-study. [8]

Air-Tight Additive Manufactured Structures

As for now there is no serious research regarding air-tight printed structures. Lunar additive manufacturing research assume an inflatable to hold the pressure [6][31]. Printed samples are often highly porous [26] [31].

2.4 Alternatives

2.4.1 Sintering of Regolith Blocks

For now only mobile sintering techniques were investigated (see Chapter 2.3.3). Another option would be to sinter regolith into blocks or bricks which could then be layered using concrete (Chapter 2.3.4) or other additional sintering. By applying pressure during the sintering process high compressive srengths can be achieved [26].

2.4.2 Regolith Bags

An easy concept could be to just burry the module with loose regolith. Due to the lower density of the regolith the shielding must be thicker and only loose regolith would require a low angle of repose [31]. Otherwise, the regolith would just fall from the structure, if the slope is too steep.

One simple option is to fill bags with regolith and pile them until the required shield thickness is achieved [42]. By pressing of the regolith or beneficial bag material choice the properties of this shielding concept could be improved [26].

Chapter 3

Requirements

Following requirements set the framework of the mission scenario (Table 3.1). The SET-XX requirements define the mission scenario and the SYS-XX requirements are system relevant requirements.
SET-01 defines the crew size of 4, which is based on the Moon Village, and the allowed working time of the crew [8]. The working time is based on the German law as the work is written in Germany. This gives a frame for a potential time investigation of the concepts.
As the location of the habitat has a direct impact on the choice of the manufacturing method, the location is fixed in SET-02 to be near the Shackelton crater rim at the lunar southpole which is the location suggested for the Moon Village [8].
SET-03 fixes the supply from Earth to once a year for time and cost considerations. It is based on the Moon Village concept [8].
As the greenhouse module will most likely be transported after the habitat, it is assumed that rovers, robotic and tugs are available for unloading and transport of equipment (SET-04) [8].
This work does not include the power infrastructure. It is assumed that sufficient power is available. However, the power consumption shall be considered in the analysis.
SYS-01 defines that in-situ resources shall be utilized. If this is not feasible, the transport cost shall be estimated and included.
The greenhouse module shall be pressurizable to hold a atmosphere that is suitable for plant growth and to connect the greenhouse module with the habitat such that the crew can easily access the module without leaving the habitat (SYS-02).
This volume shall be least 92 m^3 to be comparable with the EDEN NG design [7].
SYS-04 requires that the greenhouse module can be connected to the habitat. As no fixed habitat is available, a detailed design of the connection interface is not required but the capability of the system to interface with the habitat shall be given.

The lacking atmosphere requires a sufficient shielding of the habitat against radiation to protect humans and plants. Radiation dose thresholds differ slightly and therefore, the threshold suggested for the Moon Village of < 250 mSv per year is defined (SYS-05) [8].
Micrometeorite impacts are a threat for the modules and the crew inside as the Moon does not have an atmosphere that burns the micrometeorites before impact [9]. The requirement defined by Ceccanti et al. of a chance of no penetration by micrometeorites of 99% over 10 years is used (SYS-06) [6].
The thermal conditions on the Moon are challenging both for humans and plants [9]. Thermal insulation is required to maintain the temperature inside the greenhouse in a sufficient range. This circumstance leads to requirement SYS-07 .

Table 3.1: List of requirements for the development of the printed lunar greenhouse. They set the framework for this thesis.

SET-01	A crew size of 4 shall be assumed for operation and construction tasks. The work load shall not exceed 50% of the nominal working hours, when assuming that 50% is sufficient to perform other mandatory tasks. *Nominal working hours are driven by German law. So 8 hours per day. It can be extended to 10 hours, if the average working hours do not exceed 8 hours over six calender months. [ArbZG § 3 Arbeitszeit der Arbeitnehmer]*
SET-02	As the habitat location, a spot near the Shackelton crater rim at the southpole shall be assumed. [8]
SET-03	An annual resupply can be assumed. [8]
SET-04	It can be assumed that rovers, robotics, tugs and a mobile crane for unloading and transport purposes are available. [8]
SET-05	It can be assumed that sufficient power is available. *However, the power consumption shall be considered in the analysis.*
SYS-01	The structure and the material of the structure shall be produced on site. If smaller fractions of the total mass cannot be produced on site, the transport cost shall be determined.
SYS-02	The volume shall be pressurizable.
SYS-03	The pressurizable volume shall be at least 92 m^3. [7]
SYS-04	The greenhouse module shall provide the ability to be connected to the habitat module.
SYS-05	The system shall provide radiation shielding to achieve a dose of < 250 mSv per year. [8]
SYS-06	The system shall provide a chance of no penetration by micrometeorites of 99% over 10 years. [6]
SYS-07	The system shall provide thermal insulation.

Chapter 4

Manufacturing Method

In this chapter one manufacturing method is defined to manufacture the greenhouse module. Therefore six manufacturing methods are designed and evaluated in a trade-off analysis. The six manufacturing methods are

1. Chapter 4.2.1 - Contour Crafting with hydraulic concrete
2. Chapter 4.2.2 - Contour Crafting with sulfur concrete
3. Chapter 4.2.3 - Contour Crafting with geopolymer concrete
4. Chapter 4.2.4 - D-Shape method
5. Chapter 4.2.5 - Solar and laser sintering
6. Chapter 4.2.6 - Regolith bag method

4.1 Method

Six different ISRU manufacturing processes are designed and include the complete process chain. Required transport mass and power consumption of each method is estimated based on existing, elaborated or custom designed components. If necessary, components are scaled linear with respect to the respective capacities such as throughput capacity or chamber volume if necessary. It is assumed that the components can be scaled linear. This is not always true. However, it is done in this work due to the number of systems and time restrictions. Scaling is only done at component and not on system level to keep scaling errors lower. Margins are added according to the ESA-TECSYE-RS-006510 standard [43].
As for some methods the transport mass is directly influenced by the dimensions of the structure, a half cylinder will be defined as an assumption for the mass estimations.
The half cylinder has an inner length of 6.6 m and an inner diameter of 8.44 m

with a wall thickness of 2 m of loose regolith. As the density of loose regolith 1,500 kg m^{-3} is assumed [9]. 2 m were chosen because Ceccanti et al. state that a thickness of 1 m - 2 m is sufficient to protect life against radiation and micrometeorites [6]. This leads to a volume of 495.55 m^3 and a mass of 689,332 kg. The same mass will be assumed for solidified regolith structures.

A PUGH-matrix is used to perform a trade-off of the different processes.
Evaluation criteria are the complexity of the manufacturing process (A), the quality of the final structure (B), the complexity of the regolith processing (C), the transport mass (D) and the power consumption (E). Criteria (A) is made up of the automatisation of the process, quantity of necessary steps and critical points, which includes situations during the process that can be critical for the construction, during the manufacturing process. The quality of the final structure (B) is defined by the compressive strength as it is often the only or the main strength characteristic provided [30][26][40][32]. Criteria (C) is made up of the quantity and difficulty of necessary steps.
Each criteria is rated from one to five with one being very good and five being very bad. Each main criteria is weighted the same. Each sub criteria is weighted the same within the main criteria. The discussion includes a weighting and sensitivity analysis.

4.2 Results

4.2.1 Contour Crafting - Hydraulic Concrete

Process Chain

Figure 4.1 shows a block diagram of the manufacturing process with hydraulic concrete.
The regolith is excavated and separated by size in the sieving system. One part of the sieved regolith is used for the cement production, which includes the benification, mill and furnace. The other part is used as the agglutinate of the concrete. Cement and sieved regolith are mixed together with sieved and optionally milled water-ice rich regolith in the mixing system. The rover manufactures the structure by pushing the feed stock through a heated nozzle to melt the water-ice. Fine water-ice rich regolith is used instead of liquid water as it is significantly easier to handle. The core of the structure can be filled with either concrete, sieved and or raw regolith.

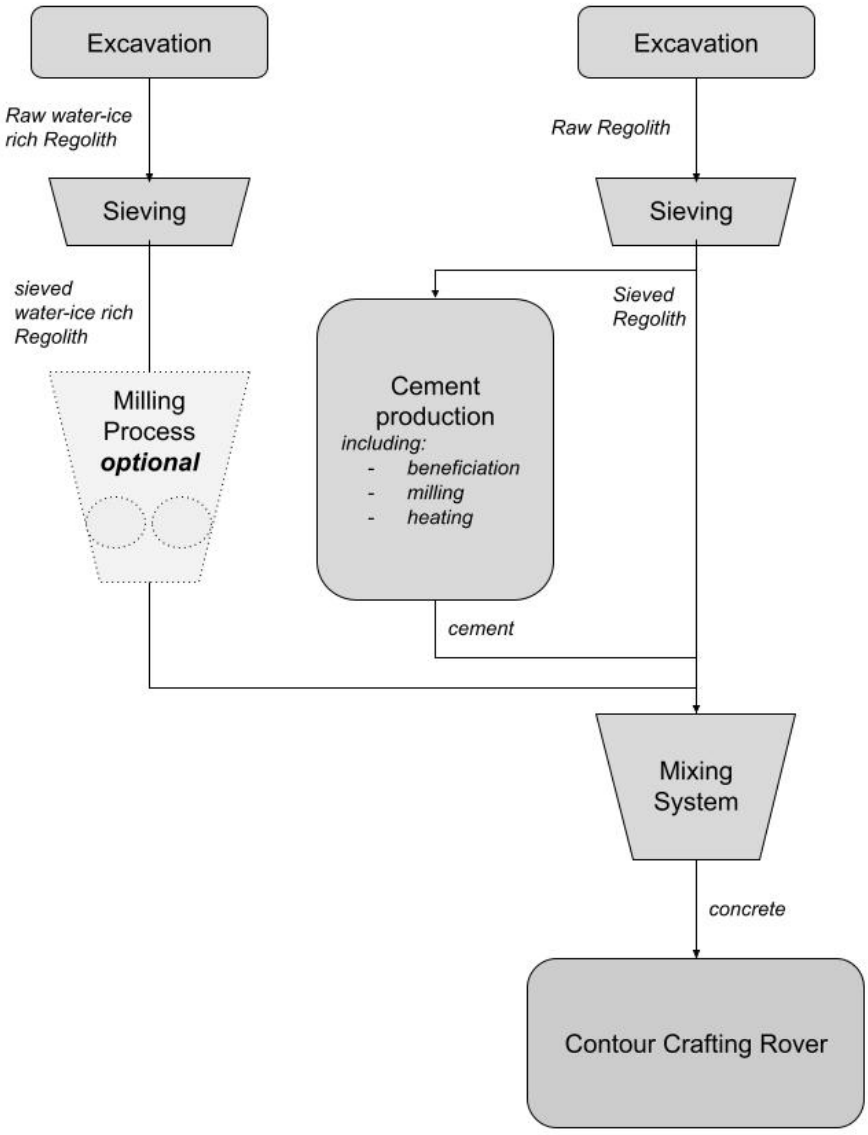

Figure 4.1: Block diagram of the contour crafting manufacturing process with hydraulic concrete. Regolith is excavated at two sites with one providing water-ice rich regolith. The water-ice rich regolith is sieved and can be optionally milled. Regolith excavated at the other site is also sieved but partially used for cement production which includes a benefication, milling and heating process. The sieved regolith, cement and water-ice rich regolith are mixed in the mixing system and loaded onto the contour crafting rover.

Excavation

The regolith excavation will be similar for all manufacturing methods. For further analysis it will rely on the RASSOR 2.0 system (see Chapter 2.3.1). It is chosen based on the analysis of Just et al. (see Chapter 2.3.1 and [12]) and its low weight per rover (66 kg), good excavation rate (min 112.5 $\mathrm{kg\,h^{-1}}$) and a relative high TRL of 4 [13]. Multiple rovers can be operated to reduce required excavation time. Based on the half cylinder described in Chapter 4.1, the excavation time with one excavation rover is roughly 255 days. This does not include the separated coarse fraction or regolith used for further processing such as the cement production. It is assumed that at least 10 rovers will be used (see Chapter 4.3.1).

Size Separation

The unprocessed regolith is separated by size with a vibration sieve as vibration sieving is a well known industrial process with high sieving rates and rather low complexity (see Chapter 2.3.2).
The Russel Compact Sieve 600 was chosen as a suitable system. It provides a continuous operation due to top-loading and bottom unloading of the material and the continuous outflow of the coarse fraction. If necessary, it is possible to change the screens easily without tools due to the clamping mechanism of the sieve. It is also possible to add a magnetic separator to the compact sieve which allows to remove material rich of iron. [44]
The Russel Compact Sieve 600 weighs 92 kg and has a power consumption of 0.3 kW [45].

Cement Production

There is currently no intensive research on on-site production of lunar cement for hydraulic concrete.

Ordinary Portland Cement is produced by crushing and heating of the four main components Calcium carbonate ($CaCO_3$), silicate (SiO_3), alumina (Al_2O_3) and iron oxide (Fe_2O_3). They are crushed, mealed and blended over a long duration and heated to form calcium silicates and aluminates. After cooling, the clinker is formed which is grounded and mixed with gypsium, limestone and or ashes to create cement. [46]

Silicia, alumina, calcium and iron oxides are minerals that can be found in lunar regolith [9]. To enrich the feed stock with these minerals before cement production, magnetic separation as described in Chapter 2.3.2 will be used. The Reading Induced Roll Magnetic Separator will be used for magnetic beneficiation. It is based on multiple rollers rotating between the poles of powerful electromagnets [47].
The system has a throughput capacity of 2,000-5,000 $\mathrm{kg\,h^{-1}}$ and is down scaled to a capacity of 1,000 $\mathrm{kg\,h^{-1}}$ [47]. This value is chosen because ten excavators

have a production rate of 1,125 kg h^{-1}. Although it is unlikely that 100% of the excavated regolith will be feed into the magnetic separator, it shall provide the capability to handle a large fraction (> 80%) of it.
This leads to a system mass of 2,400 kg and a power consumption of 2.8-3.75 kW [47]. A 20% mass margin is added.

For grinding of the feed stock ball mills, vertical roller mills, roller presses or horizontal roller mills can be used. For further mass assumptions a MTW138 vertical roller mill is used as vertical roller mills provide easier loading and unloading for this mission scenario. The MTW138 has a total mass of 29,000 kg, a power consumption of 90 kW and an output of minimum 7,000 kg h^{-1} and a maximum of 15,000 kg h^{-1} [48]. Assuming that roughly half of the excavated regolith is used for cement production, the mill is scaled down to minimum 500 kg h^{-1} with the factor 14 which leads to a mass of 2,071 kg and a power consumption of 6.43 kW. A 20 % margin is added.
For cement production a high temperature furnace is required to heat the feed stock to 1,500 °C [46]. The HTL 10/16 from ThermoConcept is chosen as a base for the trade off due to the sufficient maximum temperature of 1,600 °C [49]. It has a capacity of 10 L, weighs 97 kg and has a power of 4 kW [49]. With the assumption that the material needs to be heated for one hour, a capacity of 500 kg is required which leads to roughly 330 L of chamber volume. Scaling with the factor 33, a capacity of 330 L, a total mass of 3,200 kg and a power of 132 kW are obtained. A 20% mass margin is added.

Mixing System

The purpose of the mixing system is to achieve a homogeneous feed stock and therefore a higher quality final structure in terms of strength and porosity.
A simplified illustration is shown in Figure 4.2. A rotating part mixes the components until the desired homogeneity is reached. It will be loaded from the top and unloaded from the bottom by rotating the bottom around one axis. Therefore two electric motors are required. One to rotate the mixing part and one to unload the material. For simplicity, one motor is chosen for both purposes. The R88M-3K030C Servomotor from Omron has a rated torque of 9.55 N m, a rated speed of 3,000 min^{-1} at a power consumption of 3.48 kW and a mass of 11.5 kg [50].
A upper hopper diameter d1 of 50 cm, a bottom hopper diameter d2 of 40 cm, a hopper height h of 30 cm and a thickness t of 0.5 cm lead to a mass for an aluminum hopper of roughly 12.9 kg. Assuming that the rotary part is composed of two aluminum beams with the dimensions 38 cm x 1 cm x 1 cm, a mass of roughly 0.2 kg is estimated for the rotary part. This leads to a total mass of 31.9 kg. A 20% margin is added onto the motors and a 20% margin is added on the custom designed hopper and rotation part and the complete system.

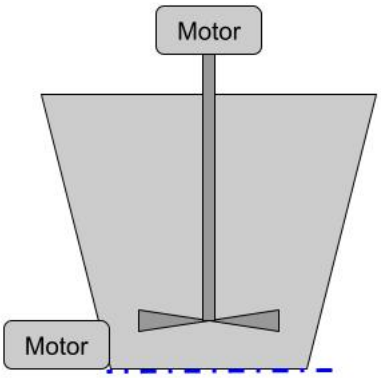

Figure 4.2: The mixing system is composed of a hopper like structure that is loaded from the top and unloaded from the bottom by rotating the bottom around the blue axis. The rotating part mixes the components. Two electric motors are used to power the rotating part and the unloading.

Contour Crafting Rover

The contour crafting rover will be similar to the rover designed by Khoshnevis et al. (Chapter 2.3.3 [30]). However, as Khoshnevis et al. do not describe the rover in detail, especially in terms of power and mass consumption, a rough model is designed for the trade-off [30].
The rover will be one tri-ATHLETE rover with a mass of 750 kg as it is assumed that one tri-ATHLETE rover provides a sufficient payload [51]. As no information is given about the power consumption, the data of the first generation will be used. Each of the six wheels of the first generation is powered by one 730 W motor [52]. As no more detail on the power consumption is given, a BLDC motor with a rated power of 750 W and a power consumption of 1100 W is used for the power estimation. This leads to a total power consumption of 3.3 kW per rover [53]. A 20% margin is added.

The heated nozzle will be powered with electric heating bands with a power of 6 $\mathrm{W\,cm^{-2}}$. As a diameter of the heating band 10 cm with a height of 10 cm is assumed which leads to a power consumption of 4.7 kW. A 20% margin is added.

As a robotic arm the CR16 robot from DOBOT will be assumed. The CR16 has six degrees of freedom and is rated with a payload of 16 kg with a total weight of 40 kg and a power consumption of 350 W [54]. Due to the lower gravity, the robot can lift weights up to 96 kg on the lunar surface. A 10% margin is added.

To push the feed stock through the nozzle, pressure needs to be built onto the material. A potential system utilizing a screw is shown in Figure 4.3. The

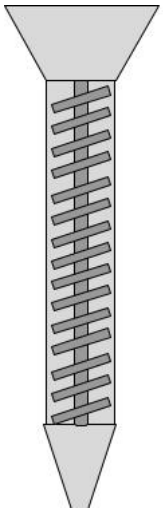

Figure 4.3: Simplified illustration of a potential feed system for the contour crafting rover. The rotating screw transports the feed stock from the upper hopper to the nozzle. The resulting pressure extrudes the feed stock through the heated nozzle.

rotating screw is designed to transport the material downwards and creating the required pressure for extrusion through the heated nozzle. For further analysis the R88M-3K030C Servomotor from Omron will be used, which has a mass of 9.4 kg, a power consumption of 239.8 W and a rated torque of 9.55 N m [50]. A 20% margin is added. The hopper on top is similar to the hopper of the mixing system with a mass of 12.9 kg whereas the nozzle with a height of 0.15 m, a radius r1 of 0.2 m, a radius r2 of 0.05 m and a thickness of 0.005 m has a weight of 1.56 kg. The cylinder with a length of 1 m, a diameter of 0.4 m and a thickness of 0.005 m has a mass of 16.75 kg. For the screw a aluminum cylinder with a diameter of 0.15 m and a length of 1 m is assumed which leads to a mass of 47.71 kg. To the hopper, cylinder, nozzle and screw a 20% margin is added. Considering an additional system margin of 20%, the feed system has a mass of 125.5 kg and a power consumption of 8.8 kW.

Mass and Power

Table 4.1 summarizes the mass and the power consumption of the contour crafting manufacturing method with hydraulic concrete.

Table 4.1: Mass and power overview of the contour crafting manufacturing process with hydraulic concrete

Process	Description	Mass [kg]	Power Consumption [kW]	Quantity	Margin	Total Mass [kg]	Total Power Consumption [kW]
Excavation	RASSOR 2.0	66	4.5	10	1.1	726	4.95
Sieving System	Russel Compact Sieve	92	0.05	1	1.1	101.2	0.055
Rover	tri-ATHLETE	750	6.6	1	1.1	825	7.26
Mixing System	Custom Design	36.1	6.96	1	1.2	43.32	7.656
Robotic	DOBOT CR16	40	0.35	1	1.1	44	0.385
Feed System	Custom Design	125.5	7.36	1	1.2	150.587	8.832
Mill	MTW138	2071	6.43	*optional*	1.2		
Benefication	IRMS	2800	3.75	1	1.2	3360	4.5
Furnace	HTL 10/16	3201	132	1	1.2	3840	158.4
Total						9090	195
Total + 20% margin						10 908	234

4.2.2 Contour Crafting - Sulfur Concrete

Process Chain

Figure 4.4 shows a block diagram of the manufacturing process with sulfur concrete.
One part of the excavated raw regolith is sieved whereas the other part is fed to the sulfur extraction unit. The pure sulfur and the sieved regolith are mixed in the mixing system with a defined sulfur content of 35% as stated in Chapter 2.3.4. The dry concrete mixture is loaded onto the contour crafting rover which manufactures the structure by extruding the dray mixture through a heated nozzle to melt the sulfur and create sulfur concrete. The core of the structure can be filled with either concrete, sieved and or raw regolith.

Excavation

These steps work accordingly to Chapter 4.2.1.

Size Separation

These steps work accordingly to Chapter 4.2.1.

Sulfur Extraction Unit

The Sulfur extraction unit is made of a high temperature furnace to extract the sulfide gasses and a sulfur recovery unit which is composed of a catalyst reactor to form the pure sulfur and a condenser to liquefy the pure sulfur.
The regolith is heated to 950 - 1,100 °C in a high temperature furnace. The KITTEC CTH500 furnace was chosen which has has a maximum temperature of 1,320 °C, a mass of 850 kg, a capacity of 500 L and a power consumption of 62.4 kW [55]. As the CTH500 is not declared as air tight or as a vacuum furnace, adaptations must be made to capture the gasses [55]. These will not be described in explicit but considered in the margin of 10%.
No suitable catalyst reactor has been found. Therefore, the mass of the K4803T condenser will be assumed for the catalyst reactor as it provides an in- and outlet and high internal volume [56]. Two pumps will pump the extracted gasses through the catalyst reactor into the condenser. As a pump, the 2660N48XNTL-SXX Thomas Oil-less WOB-L Piston Compressor / Vacuum Pump was chosen [57]. It provides a maximum open air flow of 130.3 $\mathrm{L\,min^{-1}}$ with a power consumption of 0.621 kW and a weight of 7.8 kg [57]. A 20% margin is added.
Activated Alumina will be used as the catalyst. It will be transported from Earth once as it can be regenerated by heating between 300 and 400 °C [58]. Although not filled completely during production, the volume of the catalyst reactor (K4803T condenser) will be assumed as a volume to be transported. With a density of 769 $\mathrm{kg\,m^{-3}}$ and a reactor volume of 0.1595 $\mathrm{m^3}$, the transport mass is 122.65 kg [56]. A 20% margin is added.
As a condenser, the K4803T condenser from Bitzer with a weight of 360 kg is

chosen [56]. The K4803T is a water cooled condenser [56]. However, it is not likely that water is used as a coolant. Other coolants could be cold gasses or liquid nitrogen. The condenser has a coolant volume of 45 L [56]. Assuming liquid nitrogen with a density of 808 $\mathrm{kg\,m^{-3}}$, 37 kg plus a 20% margin will be considered as a coolant mass [59].

The liquid sulfur needs to be solidified for further processing. This can be achieved by further cooling of the liquid phase.

Mixing System

It will be similar as described in Chapter 4.2.1.

Contour Crafting Rover

The contour crafting rover will be similar as described in Chapter 4.2.1.

Mass and Power

Table 4.2 summarizes the mass and the power consumption of the contour crafting manufacturing method with sulfur concrete.

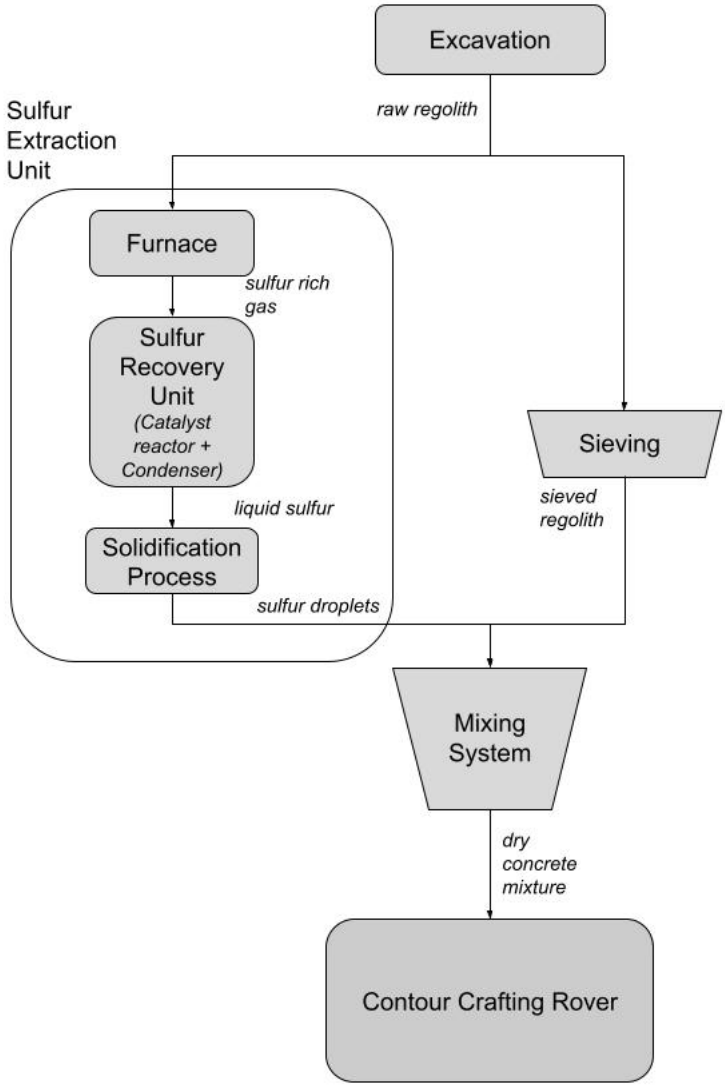

Figure 4.4: Block diagram of the contour crafting manufacturing process with sulfur concrete. One part of the excavated raw regolith is used as feed stock for the sulfur extraction unit. In a furnace the regolith is heated and the sulfur rich gas is processed in the sulfur recovery unit which is composed of a catalyst reactor and a condenser. The liquid sulfur is then solidified. The solid sulfur is mixed with sieved regolith in the mixing system and the resulting dry mixture is loaded onto the contour crafting rover.

Table 4.2: Mass and power overview of the contour crafting manufacturing process with sulfur concrete

Process	Description	Mass [kg]	Power Consumption [kW]	Quantity	Margin	Total Mass [kg]	Total Power Consumption [kW]
Excavation	RASSOR 2.0	66	4.5	10	1.1	726	4.95
Sieving System	RUSSEL Compact Sieve	92	0.05	1	1.1	101.2	0.055
Rover	tri-ATHLETE	750		6.61	1.1	825	7.26
Mixing System	Custom Design	36.1	6.96	1	1.2	43.32	7.656
Robotic	DOBOT CR16	40	0.35	1	1.1	44	0.385
Feed System	Custom Design	125.5	7.36	1	1.2	150.587	8.832
Condenser	K4803T + 2660N48XNTLSXX + coolant	412.8	0.621	1	1.2	485.76	0.7452
Catalyst reactor	K4803T + 2660N48XNTLSXX	367.8	0.621	1	1.2	441.36	0.7452
Catalyst	activated alumina	154	-	1	1.2	184.8	-
Furnace	KITTEC CTH 500	850	62.4	1	1.1	935	68.64
Total						3937	103
Total + 20% margin						4724	124

4.2.3 Contour Crafting - Geopolymer Concrete

Process Chain

Figure 4.5 shows a block diagram of the manufacturing process with geopolymer concrete. Regolith is excavated at two different sites with one providing water-ice rich regolith. Both raw materials are sieved and mixed in the mixing system. One part of the dry sieved regolith is enriched with magnesium oxide (MgO) by magnetic separation. The created MgO rich powder is also mixed with the other two components into a homogeneous MgO and water-ice rich regolith mixture which is loaded onto the contour crafting rover. The rover manufactures the structure by pushing the dry feed stock through the heated nozzle which leads to the melting of the water ice and therefore the forming of a one-part geopolymer. The core of the structure can be filled with either concrete, sieved and or raw regolith. The structure is then cured.

Excavation

These steps work accordingly to Chapter 4.2.1.

Size Separation

These steps work accordingly to Chapter 4.2.1.

Alkali Activator Production

As stated in Chapter 2.3.4, MgO is a suitable alkali activator for a one-component geopolymer. It can be beneficiated by magnetic separation due to its non-magnetic properties. The system will be similar to the system described in Chapter 4.2.1.

Mixing System

It will be similar as described in Chapter 4.2.1.

Contour Crafting Rover

The contour crafting rover will be similar as described in Chapter 4.2.1.

Curing

There is no generic perfect curing scheme identified for geopolymer concrete. A complex trade-off is necessary which will not be part of this work. For the trade-off, it will be assumed that the structure is cured in local environment conditions and no additional structure and or system is needed.

Mass and Power

Table 4.3 summarizes the mass and the power consumption of the contour crafting manufacturing method with geopolymer concrete.

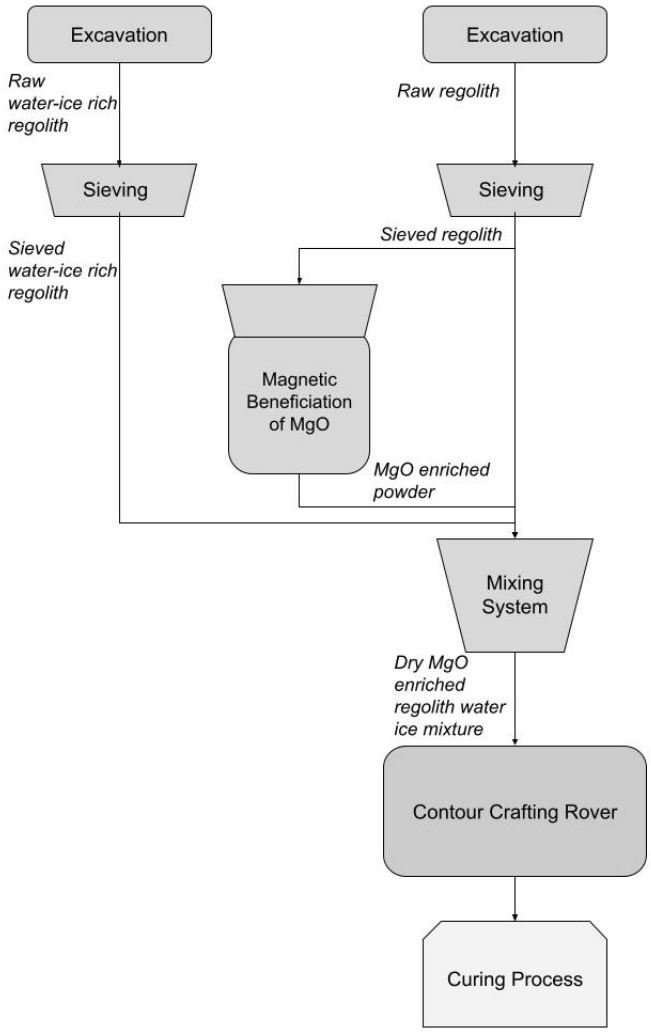

Figure 4.5: Block diagram of the contour crafting manufacturing process with geopolymer concrete. Similar to the hydraulic concrete, the regolith is excavated at two sites of which one procides water-ice. The raw dry regolith is sieved and one part is used as feed stock in a magnetic benefication of MgO to obtain MgO enriched powder which is mixed with the sieved water-ice rich and the dry sieved regolith in the mixing system. The mixture is loaded onto the contour crafting rover.

Table 4.3: Mass and power overview of the contour crafting manufacturing process with geopolymer concrete

Process	Description	Mass [kg]	Power Consumption [kW]	Quantity	Margin	Total [kg]	Total Power Consumption [kW]
Excavation	RASSOR 2.0	66	4.5	10	1.1	726	4.95
Sieving System	RUSSEL Compact Sieve	92	0.05	1	1.1	101.2	0.055
Rover	tri-ATHLETE	750	6.6	1	1.1	825	7.26
Mixing System	Custom Design	36.1	6.96	1	1.2	43.32	7.656
Robotic	DOBOT CR16	40	0.35	1	1.1	44	0.385
Feed System	Custom Design	125.5	7.36	1	1.2	150.587	8.832
Benefication	IRMS	2800	3.75	1	1.2	3360	4.5
Total						5256	37
Total +20% margin						6300	44

4.2.4 D-Shape

Process Chain

Figure 4.6 shows a block diagram of the D-Shape manufacturing process. For the ink production, water is extracted in a thermal water extractor and mixed with dry salts in a mixing system. The ink is then fed into the spraying head of the D-Shape rover. For the dry feed stock, unprocessed excavated regolith is sieved and then enriched with magnesium oxide (MgO). The enriched and sieved regolith is loaded onto the printing head of the rover. Once fully loaded, the rover layers the dry feed stock with the printing head and injects the liquid ink into the layer.

Excavation

These steps work accordingly to Chapter 4.2.1.

Size Separation

These steps work accordingly to Chapter 4.2.1.

MgO Benefication

As stated in Chapter 2.3.3 a magnesium oxide content of 25 wt.% is necessary and as the regolith samples indicate a lower concentration, a magnesium oxide benefication step is necessary [31] [9].
Due to the non-magnetic properties of pure MgO, magnetic separation methods are suitable for this benefication step. It will be similar to the system described in Chapter 4.2.1.

Thermal Water Extractor

A thermal water extractor that will be used for a real mission will be a complex system as stated in Chapter 2.3.2. This system will be simplified for the trade off to a furnace to sublimate the water ice and a condenser to liquefy the water vapor. Similar to the Sulfur Extraction Unit the KITTEC CTH500 furnace and the K4803T condenser including the 2660N48XNTLSXX Vacuum Pump by Gardner Denver are used for the trade-off which leads to a system mass of 1,217.8 kg and a power consumption of 63 kW (see Chapter 4.2.2).

Ink Mixing System

The purpose of the ink mixing system is to create a water/$MgCl$ mixture of desired $MgCl$ concentration. The dry salts are mixed with liquid water to form the liquid binder.
As it includes the handling of a liquid in a vacuum environment, adaptations to the prior mentioned mixing system must be made. It shall be air tight and either the temperature and or the pressure is controlled. However, the mass and

power estimations as described in Chapter 4.2.1 are assumed.
The liquid ink will most likely be stored in a pressurized tank which can be connected to the rover with a quick connection. The $MgCl$ salt will be transported from Earth. Cesaretti et al. estimate a total of 3,800 kg dry salt for a shell of 250,000 kg [31]. Assuming the model cylinder as described in Chapter 4.1, the transport mass of the salt would add to 10 477.85 kg to which a 20% margin is added.

D-shape Rover

Similar to the contour crafting rover, the D-Shape system will be mounted on a 'ATHLETE' rover. Main components of the printing system are the printing head, which layers the dry MgO rich regolith, the spraying head, which injects the liquid ink into the dry layer, a feeding system for both heads and a robotic arm to move the spraying and printing head.
A big challenge is to design the spraying head and the feed system to work in vacuum conditions. The spraying head itself shall drop the inorganic binder into the layered sand without drastic decrease of the system pressure. The whole system needs to be insulated or even heated due to the low temperatures on the Moon to keep the binder in the liquid phase.

The printing head must be designed to prevent clogging. For the trade-off, the spraying head will be assumed as a vibration feeder including a hopper for feed stock storage and a trowel following the feeder to evenly spread the dry material (see Figure 4.7). The hopper is similar to the one used for the mixing system. A motor opens the bottom of the hopper from which the regolith (orange arrow) falls onto the conveyor belt which transports the feed stock onto the construction side by vibration. A following trowel smoothens out the regolith. The HVL 8/2 vibration motor from Vibra Schultheis will be used. It has a mass of 12 kg, a power consumption of 0.54 kW and a rated speed of 2,850 min^{-1} [60]. For the mass estimation the DOBOT FBAND is assumed for the conveyor belt. It has a weight of 4.2 kg [61]. The trowel is assumed to be a simple 0.5 m x 0.05 m x 0.005 m aluminum blade with a mass of 0.34 kg. This leads to a system mass of 38.84 kg and a power consumption of 4.22 kW for the printing head/feed system. Considering a margin of 10% for both motors, 10% for the conveyor belt and 20% for the trowel and hopper and the complete system, the system mass with margin is 51.564 kg with a power consumption of 5.064 kW. A 20% margin is added to the feed system.

The spraying head consists mainly of an injector nozzle, a small pump to control the flow of the liquid ink and the feed system including the tank described in the Ink Mixing System section. The pump will be a small electric oil-pump with a mass of 3 kg, a power consumption of 0.06 kW and a delivery rate of 1 $\text{L}\,\text{min}^{-1}$ [62]. The Reliance – Aquasystem 12 Litre Potable Expansion Vessel XVES050040 will be assumed as a tank. It weighs 0.65 kg and is rated to a maximum pressure of 10 bar [63]. The supply section of the feed system will

be considered in the margin and not further designed here. It is most likely that the injector nozzle will be designed in house to meet all not yet defined requirements, but it is assumed that it will not exceed a mass of 0.1 kg.

The robot arm will be similar as described in Chapter 4.2.1.

Mass and Power

Table 4.4 summarizes the mass and the power consumption of the D-shape method.

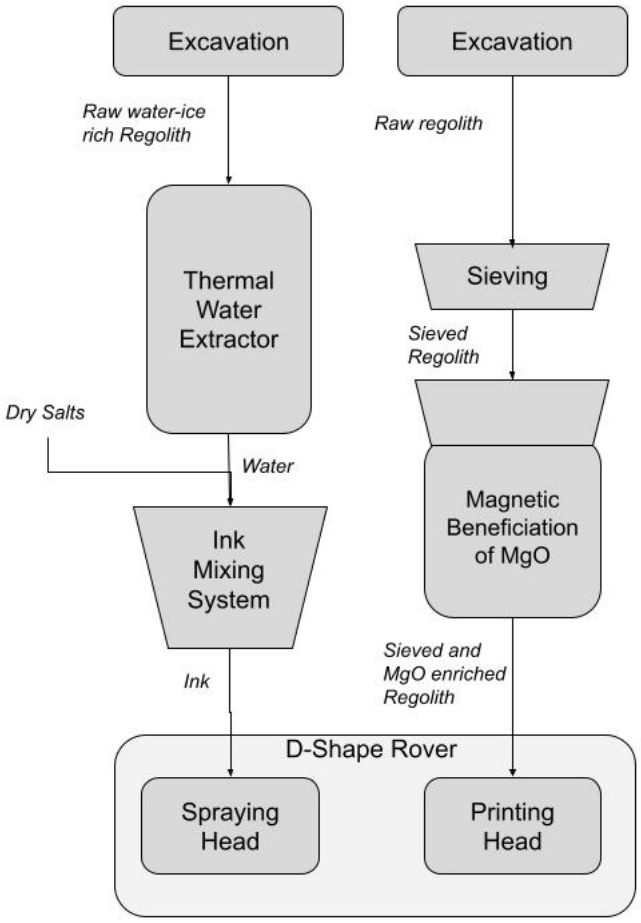

Figure 4.6: Block diagram of the D-Shape manufacturing process. Water-ice rich regolith is excavated at one site and the water is extracted in a thermal water extractor and mixed with the dry salt magnesium chloride($MgCl$) in the ink mixing system. The liquid ink is stored and connected with the spraying head. The regolith excavated at the other site is sieved and enriched with MgO by magnetic benefication and loaded onto the printing head of the D-shape rover.

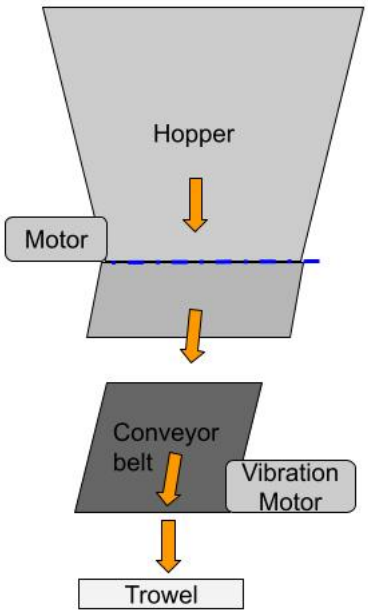

Figure 4.7: Regolith feed system with a storage hopper which is unloaded from the bottom onto a vibration conveyor belt. The orange arrows show the flow of the regolith. A trowel spreads the regolith evenly.

Table 4.4: Mass and power overview of the D-shape method. The mass of dry salt is estimated with the model half cylinder and

Process	Description	Mass [kg]	Power Consumption [kW]	Quantity	Margin	Total [kg]	Total Power Consumption [kW]
Excavation	RASSOR 2.0	66	4.5	10	1.1	726	4.95
Sieving System	RUSSEL Compact Sieve	92	0.05	1	1.1	101.2	0.055
Rover	tri-ATHLETE	750	6.6	1	1.1	825	7.26
Mixing System	Custom Design	36.1	6.96	1	1.2	43.32	7.656
Robotic	DOBOT CR16	40	0.35	1	1.1	44	0.385
Feed System	Custom Design	51.564	4.22	1	1.2	61.877	4.624
Benefication	IRMS	2800	3.75	1	1.2	3360	4.125
Furnace	KITTEC CTH 500	850	62.4	1	1.1	935	68.64
Condenser	K4803T + 2660N48XNTLSXX + coolant	412.8	0.621	1	1.2	485.76	0.6831
Ink storage + spraying head	Reliance Vessel XVES050040 + Pump + Injector	3.75	0.06	1	1.2	4.5	0.0721
Dry salt	$MgCl$	10 477.85	-	1	1.2	12 573.42	-
Total						19 166	103
Total + 20% margin						22 992	124

47

4.2.5 Sintering

Process Chain

Figure 4.8 shows a block diagram of the sintering process.
The excavated regolith is sieved and directly loaded into the feed system of the sintering rover. After each new layer of fine regolith is distributed by the feed system, the energy beam is moved onto the layer of regolith. A new layer is then disposed.
Two different types of energy sources for the beam are considered. The first one is the solar sintering approach in which the direct sun light is concentraded and the second one is laser sintering in which a laser is used.

Excavation

These steps work accordingly to Chapter 4.2.1.

Size Separation

These steps work accordingly to Chapter 4.2.1.

Laser Sintering Rover

The laser sintering rover is composed of the ATHLETE rover, a regolith feed system, a robotic arm and the laser system.
The robotic arm (see Chapter 4.2.4) moves the laser system which consists of ten 40 W $DC - CO_2$ laser cutter [64]. Ten laser will be used as described by Farries et al. to increase the sintered width of the system [32]. This leads to

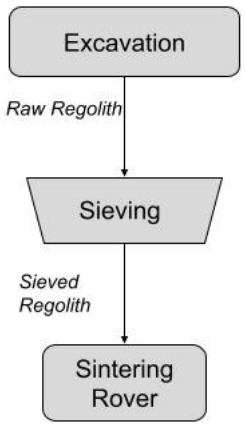

Figure 4.8: Block diagram of the sintering manufacturing process. Raw regolith is excavated, sieved and loaded onto the sintering rover.

a power consumption of 6.24 kW for the laser and a mass of 68 kg to which a 10% margin is added. [64]
The feed system is similar to the one described in Chapter 4.2.4

Mass and Power

Table 4.5 summarizes the mass and the power consumption of the laser sintering method.

Table 4.5: Mass and power overview of the laser sintering process

Process	Description	Mass [kg]	Power Consumption [kW]	Quantity	Margin	Total [kg]	Total Power Consumption [kW]
Excavation	RASSOR 2.0	66	4.5	10	1.1	726	4.95
Sieving System	RUSSEL Compact Sieve	92	0.05	1	1.1	101.2	0.055
Rover	tri-ATHLETE	750	6.6	1	1.1	825	7.26
Robotic	DOBOT CR16	40	0.35	1	1.1	44	0.385
Feed System	Custom Design	51.564	4.22	1	1.2	61.877	4.624
Energy beam	Diamond C40 laser	6.8	6.24	10	1.1	74.8	8.864
Total						1833	24.156
Total + 20% margin						2199	28.9872

Solar Sintering Rover

The solar sintering rover is composed of the ATHLETE rover, a fresno lense, a mirror, one robotic arm to move the fresno lense in required direction, one robotic arm to move the mirror to redirect the sun light in required direction onto the fresno lense and a regolith feed system.
The robotic arm is the CR16 as described in Chapter 4.2.1.
Urbina et al. state that a fresnel lense powerful enough would only weigh 2 kg [33]. A 20% margin is added to this mass. For the mirror the same mass as the fresno lense is assumed and a 20% margin is added.

Mass and Power

Table 4.6 summarizes the mass and the power consumption of the solar sintering method.

Table 4.6: Mass and power overview of the solar sintering method.

Process	Description	Mass [kg]	Power Consumption [kW]	Quantity	Margin	Total [kg]	Total Power Consumption [kW]
Excavation	RASSOR 2.0	66	4.5	10	1.1	726	4.95
Sieving System	RUSSEL Compact Sieve	92	0.05	1	1.1	101.2	0.055
Rover	tri-ATHLETE	750	6.6	1	1.1	825	7.26
Robotic	DOBOT CR16	40	0.35	2	1.1	44	0.385
Feed System	Custom Design	51.564	4.22	1	1.2	61.877	4.624
Energy beam	fresnel lense	2	-	1	1.2	2.4	-
	mirror	2	-	1	1.2	2.4	-
Total						1807	15
Total + 20% margin						2168.4	18

4.2.6 Regolith Bags

Process Chain

Figure 4.9 shows the process chain for regolith shielding manufacturing using regolith bags. The excavated regolith is unloaded into a hopper from which the regolith falls into attached bags. A rover closes the bags, loads them onto the rover and piles them at the construction site. A sieving step can be implemented optionally. This process requires a more active supervision by the crew due to the more difficult layering of the bags as they can have different shapes especially under different load cases which is complex to predict by artificial intelligence. The inflatable must be pressurized during construction to hold the regolith bags.

Excavation

These steps work accordingly to Chapter 4.2.1.

Size Separation and Bag Filling

A size separation can be optional included according to Chapter 4.2.1, but will not be considered for the trade-off.
The regolith is unloaded into a hopper at which bottom polyethylene bags are attached by the robotic arm of the rover. As a hopper a simple three leg aluminum hopper with a weight of 22 kg is assumed. The hopper is already

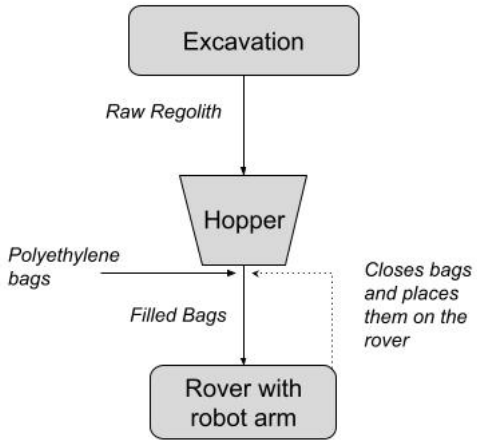

Figure 4.9: Block diagram of the manufacturing process using regolith bags. The excavated regolith is filled into the polyethylene bags via a hopper. The robotic arm on the rover closes the bags and loads it into the rover.

described in Chapter 4.2.1 and the three legs are assumed to have a height of 1.5 m and a diameter of 0.03 m.
700 L KMF-Entsorgungsbeutel (artificial mineral fiber garbage bags) are chosen. They are used for carcinogenic fibre trash and provide good punctual resistance at a light weight of 0.26 kg [65]. Polyethylene also provides additional radiation shielding due to the high hydrogen content in the compound [37]. Based on the model half-cylinder (see Chapter 4.1) and the conservative assumption that the bags can be filled to only 50%, 1313 bags are required.

Regolith Bag Rover

The rover for the regolith bag process is composed of a KUKA KR 300 R2700-2 six axis robot arm and the tri-ATHLETE rover.
For the decision on a robot arm the requirement was defined to provide the ability to handle a full 700 L bag of regolith. Assuming the density of loose regolith (1,500 $\mathrm{kg\,m^{-3}}$) the mass of one bag would be 1,050 kg. Considering the lower gravity, the KUKA KR 300 has a more than sufficient payload capacity of 300 kg and a total mass of 1,101 kg [66]. There is no information about the power consumption of the robot arm. Therefore, the power consumption of the DOBOT CR16 which is used for the other manufacturing methods, will be scaled. Scaling with respect to the system mass leads to a power consumption of 9.625 kW while scaling with respect to the payload mass a power consumption of 6.475 kW is calculated. For the trade-off the higher value is chosen.
The tri-ATHLETE payload capacity is sufficient to carry the robot arm and one full regolith bag, as both combined have a mass of 2,151 kg and the tri-ATHLETE rovers payload capacity is 500 kg which is sufficient considering the lower lunar gravity [51]. Additional rovers could be used to transport more than one full regolith bag.

Mass and Power

Table 4.7 summarizes the mass and the power consumption of the regolith bag method.

Table 4.7: Mass and power overview of the regolith bag method

Process	Description	Mass [kg]	Power Consumption [kW]	Quantity	Margin	Total [kg]	Total Power Consumption [kW]
Excavation	RASSOR 2.0	66	4.5	10	1.1	726	4.95
Hopper	Custom Design	22	-	1	1.2	26.4	-
Rover	tri-ATHLETE	750	6.6	2	1.1	1650	7.26
Robotic	KUKA KR 300 R2700-2	1101	9.625	1	1.1	1211.1	10.5875
Bags	KMF Entsorgungsbeutel	0.26	-	1314	1.2	409.97	-
Total						4023	23
Total + 20% margin						4828	28

4.3 Discussion

The discussion includes the trade-off analysis to evaluate the investigated methods and find the most suitable one. After a brief critical view on the trade-off analysis a weighting analysis is performed. The mass estimations are then reviewed and open issues declared. An outlook with respect to the manufacturing method is given.

4.3.1 Excavation

Just et al. [12] criticize the research status of excavation systems at that time. They are stating that current projects are lacking available information, maturity (TRL < 4) and overall only little research is done. As one reason they argue that the processing techniques are currently not mature enough to define requirements that can be cascaded to the excavated material. [12]
This may indicate that future research on lunar excavation has the potential to improve significantly.

4.3.2 Trade-Off

Table 4.8 shows the PUGH matrix of the process trade-off. All criteria are weighted the same (0.2) and all sub-criteria are weighted the same within the criteria. The scale goes from one for very good to five for very bad.

As mentioned in Chapter 4.1, the complexity of the manufacturing process is divided into degree of automatisation, steps and critical points during the manufacturing process.
All additive manufacturing processes are highly automated. The manufacturing is computer controlled and only needs minor supervision of the surface crew. Although a less complex task, the placement of the regolith is harder to automate. The reason is that the bags are not rigid and can change their form once placed or loaded burried under other bags. This requires high supervision or even remote placing by the surface crew.
The regolith bag concept only has the step to place the bags. All three contour crafting methods require to lay down the concrete and to fill the core, the sintering and D-Shape methods need to layer the dry material and then bond them.
The dependency on solar light is a major critical point for the solar sintering method. Gläser et al. report that the illumination near the Shackelton crater rim is $> 70\%$ [67]. Additionally, the low angle of incidence creates long shadows. A careful construction planning is required to mitigate the risk of being shadowed during manufacturing.
As the ink used for the D-shape method is liquid, handling and injection into the layered regolith mixture is difficult. Cesaretti et al. state that it may be possible under certain conditions (see Chapter 2.3.3 and [31]). The presence of water in form of water-ice that is melted in the contour crafting method with

hydraulic and geopolymer concrete is also critical. For the regolith bag method it is necessary to pressurize the inflatable during construction to hold the bags. As this leads to a period of the inflatable being unshielded, a potential risk of damage is raised.

Hydraulic concrete can reach compressive strengths between 36 and 67 MPa [68], whereas sulfur concrete can reach up to 35 MPa [37] and geopolymer between 5 and 80 MPa [36] depending on the curing scheme.
Khoshnevis et al. [23] have presented that sulfur concrete has reached up to 27 MPa in their contour crafting experiments with sulfur concrete. No testing was done with hydraulic or geopolymer concrete. As the extrusion pressure is a driving factor for the material properties it is assumed that all concretes will have a quite similar compressive strentgh with the contour crafting process. [23]
Cesaretti et al. have shown that the final compressive strength of structure manufactured with the D-shape process can reach compressive strengths of up to 20.35 MPa [31]. Meurisse et al. were only able to reach 2.31 MPa in their solar sintering experiments [26]. Farries et al. state that laser sintered regolith can reach compressive strengths between 4.2 and 50 MPa depending mainly on the powder density, laser power and material properties [32]. Regolith bags are filled with loose regolith and therefore have a bad compressive strength.

The D-shape and the contour crafting processes include multiple processing steps which increases the complexity and risk of failure in the process chain. Both sintering processes only require sieving of the excavated regolith, whereas no additional processing step is mandatory for the regolith bag process.
Sieving is a well known process step on Earth. However, the lower gravity might be a problem which needs further research. The hydraulic concrete approach has many open points in the regolith process chain including water-ice handling and especially the cement production which is a very complex process and benefication processes. This is also true for the sulfur and geopolymer concrete processing.
Another open point is the solidification of the liquid sulfur which is discussed in Chapter 4.3.4.

The mass estimations of each manufacturing process are shown in Tables 4.1-4.7. Main driver for the mass are the regolith processing steps. For the regolith bag process the main driver is the heavy robot arm and the second rover.

The power estimations of each manufacturing process are shown in Tables 4.1-4.7. As it directly utilizes the solar light, the solar sintering process consumes the least amount of power. Similar to the transport mass, the main driver of the power consumption is the regolith processing leading to a higher power consumption by a factor of 5 compared to solar sintering. The ten lasers of the sintering process lead to a roughly 60% higher power consumption.

Laser sintering (2.0) is the best performing manufacturing method according to the PUGH matrix (see Table 4.8). Solar sintering is performing slightly worse (2.167). Contour crafting with geopolymer concrete (2.633) and the regolith bag method (2.6) are performing almost similar. Contour crafting with sulfur (3.166) and contour crafting with hydraulic concrete (3.633) are perfoming the worst. Therefore, laser sintering is the manufacturing method used to construct the regolith shielding. It can potentially also be used to manufacture the regolith shielding of the complete habitat.

Table 4.8: PUGH matrix of the manufacturing method trade-off. All main criteria are weighted the same. All sub criteria are weighted the same within the main criteria. The shown total values are weighted accordingly.

Main criteria	Sub criteria	CC hydraulic concrete	CC sulfur concrete	CC geopolymer concrete	D-Shape	Solar sintering	Laser sintering	Regolith bags
Complexity Manufacturing process	Automatisation	2	2	2	2	2	2	2
	Steps	3	3	3	3	2	2	1
	Critical Points	3	2	3	4	3	2	2
Quality of final structure	Compressive strength	1	1	1	1	4	2	5
Complexity regolith processing	Steps	5	4	3	5	2	2	1
	Open Points	4	4	4	4	1	2	1
Transport mass		5	4	4	5	2	2	3
Power consumption		5	5	2	5	1	2	2
Total		3.633	3.266	2.633	3.7	2.167	2	2.6

Critical View on Trade-Off Analysis

In the prior trade-off it is assumed that a higher automatisation is better. This view may be questioned as a higher degree of automatisation increases the software complexity and therefore also the complexity of the manufacturing process. The software complexity was not investigated in this thesis. Therefore, a higher degree of automatisation is viewed better from crew perspective.

Although performing better in the trade-off, the scores of laser sintering and solar sintering are rather close. Small changes of the ratings lead to minor advantages for one of the sintering methods. By reducing the rating for the 'compressive strength' from 4 to 3 for solar sintering, the total rating reduces to 1.97. Reason for this adaption could be new test data of regolith samples created using solar sintering. Both systems need to be designed further to make a final decision. A weighting analysis (see Chapter 4.3.2) is performed to investigate the impact of an adapted weighting.

That the inflatable needs to be pressurized during construction and the complete mission is not only a risk for the construction. Pressure fluctuations or pressure losses due to technical failure may lead to a collaps of the structure. Intensive analysis of this risk would be necessary. However, this was not considered in the trade off as it only considered the manufacturing method and not design related risks.

Weighting Analysis

For now, all criteria were weighted the same. The analytical hierarchy process is used to investigate the influence of the weighting W. Table 4.9 shows the matrix of the analytical hierarchy process and the weighting factor W. The mass of the manufacturing method is the highest weighted criteria, as it is the parameter used for the cost-benefit analysis. It is followed by the complexity of the method and the regolith processing as they are significant criteria to identify points of failure and general feasibility. Power consumption and the quality of the final structure are weighted the lowest. The quality is weighted so low as the comparability with the regolith bag method is not given because of the different construction method. The power consumption is weighted lower as the requirement SET-05 defines that sufficient power is available. The weighting factors from Table 4.9 produce the following trade-off results:

1. Laser Sintering (2)
2. Solar Sintering (2.01)
3. Regolith Bags (2.35)
4. Contour Crafting - Geopolymer Concrete (3.27)
5. Contour Crafting - Sulfur Concrete (3.5)

Table 4.9: Matrix of the analytical hierarchy process. The mass of the manufacturing method is weighted the highest followed by the complexity of the method and the regolith processing. Power consumption and the quality of the final structure are weighted the lowest.

	Complexity Manufacturing Process	Quality	Complexity Regolith Processing	Mass	Power	Weighting factor W
Complexity Manufacturing Process	1	1	1	1/3	1	0.234
Quality	1/5	1	1/5	1/5	1	0.058
Complexity Regolith Processing	1	1	1	1/3	1	0.234
Mass	3	5	3	1	3	0.409
Power	1/5	1	1/5	1/3	1	0.065

6. Contour Crafting - Hydraulic Concrete (4.1)
7. D-shape (4.18)

Solar sintering and the regolith bag method perform better with these weighting factors as the quality of the final strucure is weighted less and the complexity of the regolith processing and the transport mass are weighted more. All manufacturing methods with complex and intensive regolith processing perform worse with this weighting. That the solar sintering method is performing similar as the laser sintering method with the adapted weighting indicates that further investigation with more advanced system designs and test data is necessary.

4.3.3 Assessment of Estimations

The process to choose one specific component for the trade-off was to define a requirement, such as the payload of a robot arm, and to look for candidates. Mandatory information are mass and power consumption. Candidates without these information were not considered. This led often only to one or two candidates. An evaluation between different candidates was not performed.
All estimations of already available commercial components include a margin of 10% as modifications are expected because the functionality in a lunar environment was not considered in the choice of components. Torques, payloads and flow capacities are all Earth rated and do not consider the lower gravity and temperature ranges on the Moon. Due to lacking information on how parameters of off the shelves component were tested, no well-founded statement can be given here. Especially the functionality of gravitational sieving in lunar gravitation consitions must be further investigated.

Custom designed components such as the hopper or custom designed systems such as the feed system are only simplified. They include a 20% margin on

component and system level. The choice of aluminum for all custom designed components must be questioned. It is used due to the low weight, but not evaluated regarding strength or stability against the large temperature ranges. However, due to it's availability on the Moon, it could be extracted on site [9].

Some sources provide equations to calculate system masses. Christiansen et al. [18] provide an equation to estimate the system mass of an IRMS. An IRMS with a throughput of 1,000 $\mathrm{kg\,h^{-1}}$ and a five stage roll system would have a calculated mass of 1,043 kg and a power consumption of 1.302 kW whereas a PRMS would have a calculated mass of 319 kg and a power consumption of 0.196 kW. [18]
Comparing this with the down scaled IRMS from Reading with a mass of 2,400 kg and a power consumption of 2.8-3.75 kW shows a significant difference between theoretical estimated properties and properties scaled based on commercial available components [47].

However, all margins should cover the uncertainties and unknowns.

4.3.4 Open Issues

The pure sulfur extracted in the sulfur extraction unit is in liquid form and a process step to solidify the liquid sulfur is needed. To create a fine sulfur powder gas atomisation may be used. Gas atomisation is a common process to manufacture aluminum powder for solid rocket motors [69].
Unal [69] states that it is a highly automated process. Melted metal is transported through a delivery tube to the atomising nozzle at which it gets in contact with the high velocity flow of the amtomising gas and forms a jet which can be either directed vertical upward, downward or horizontal. The atomising gas, which can be either nitrogen, argon or helium, can be recycled after the process. [69]
This process was not considered due to time restrictions.

4.3.5 Outlook - Manufacturing Method

Next steps would be to further design the solar and laser sintering processes to make a final decision between both methods. This may already include the design and testing of demonstrators starting with the subsystems. Retrieving the achievable material properties and respective conditions such as beam power or sinter speed are not only needed for development of the rover system but for the design of the regolith structure and the complete mission scenario and timeline.
Once fixed, the interfaces in the process chain should be investigated to design the manufacturing process in more detail.

Chapter 5

Design

In this chapter the greenhouse module is designed including the primary and secondary structure. A FEM analysis is performed to evaluate the primary structure.

5.1 Method

Based on the results of the trade-off analysis and the EDEN NG requirements a conceptual design of the primary structure is developed. This includes a CAD-model and a brief FEM analysis.
Two load cases are investigated. The regolith structure needs to hold itself and withstand gravitational forces with (Case 1) and without (Case 2) the internal pressure of the inflatable (0.1 MPa).

As a base material, concrete from the Ansys library with the properties shown in Table 5.1 (40 MPa compressive ultimate strength) was chosen. The compressive ultimate strength of regolith sintered with SLM varies between 4.2 MPa and 50 MPa depending on parameter such as laser power or powder density [32]. The compressive strength achieved with solar sintering is 2.31 MPa [26]. As most literature only give the compressive strength, the tensile ultimate strength and the youngs' module are scaled with respect to the compressive ultimate strength of 4 MPa and 10 MPa. The density was increased to 3,000 $\mathrm{kg\,m^{-3}}$ according to [8]. The FEM analysis was performed with Ansys2023.

Then the assembly and outfitting process of the module is considered.

63

5.2 Results

5.2.1 Primary Structure

Inflatable Structure

As described in Chapter 2.3.5, the inflatable is composed of the inner liner made of meta aramid, the bladder separation layer and the air containment bladder which is made of CEPAC HD200. This leads to an areal density of $\rho_{infl} = 3.08\ \mathrm{kg\,m^{-2}}$ [8].

The inflatable is a cylinder with a diameter of 4.4 m, a length of 6.6 m and a spherical end (Figure 5.1) which leads to a weight of $m_{infl} = 385.34$ kg. A 20% margin is added.

Adapter Ring

To connect the flexible inflatable with the most likely rigid habitat, an adapter ring is used. It is a simple aluminum disk with a diameter of 4.5 m and a thickness of 0.1 m and a door shaped cut out for entrance. The adapter ring will also provide necessary interfaces for connection to the habitat but as the habitat design is not fixed, it will not be part of this design. The EDEN NG project uses the Common Berthing Mechanism [7].
The inflatable will be fixed with clamps to distribute the necessary clamping force over a larger area which are realised here with cut-outs to hold the inflatable. The total mass is 3,684.43 kg. A 20% margin is added.
Figure 5.1 shows the inflatable with the adapter ring.

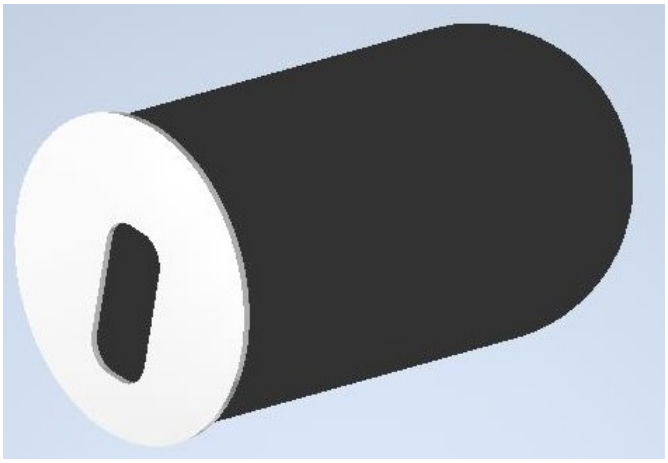

Figure 5.1: Inflatable made of CEPAC HD200 and the aluminum adapter ring.

Regolith Structure

Figure 5.2 shows the design of the regolith shielding. The minimum thickness of the shielding is 1 m as the 2 m wall made out of loose regolith with a density of 1,500 $\mathrm{kg\,m^{-3}}$ as described in Chapter 4.1 reduces to 1 m with sintered regolith and a density of 3,000 $\mathrm{kg\,m^{-3}}$ [8]. The wider bottom was chosen for easier construction and for a more stable structure.

FEM Analysis

Table 5.1 shows the scaled material properties as described in Chapter 5.1.

The mesh (see Figure 5.3) is generated using the sizing method with an element size of 0.2 m for the inner cylinder and 0.4 m for the rest of the structure. The elements are tetrahedral elements of second order.

It is assumed that the inflatable sits perfectly on the inner surface of the regolith structure. And it is simulated by a surface pressure of 0.1 MPa.
The lunar gravity is simulated by an acceleration downwards of 1.62 $\mathrm{m\,s^{-2}}$ [9] and the module is fixed at the bottom via a fixed support (see Figure 5.4).

The maximum shear, compressive and tensile stress are shown in Figure 5.5 & 5.6 with internal pressure and in Figure 5.7 & 5.8 without internal pressure and listed in Table 5.2. Both shear and tensile stresses have a maximum at the inner cylinder at the front side right above the point where the wall thickness increases. The maximum shear stress is 0.224 MPa and the maximum tensile stress is 0.349 MPa. The compressive stress is the highest at the inner surface with the maximum of 0.104 MPa located at the bottom of the structure. All three stresses are significantly (> factor 6) lower without the internal pressure (see Figure 5.7 & 5.8). The maximum shear stress is 0.02 MPa, the maximum

Table 5.1: Physical properties of concrete from the Ansys library and scaled w.r.t. the compressive ultimate strength.

Property	Concrete Ansys Lib.	Concrete scl. 1/10	Concrete scl. 1/4
compressive ultimate strength	40 MPa	4 MPa	10 MPa
tensile ultimate strength	5 MPa	0.5 MPa	1.25 MPa
density	2,300 $\mathrm{kg\,m^{-3}}$	3,000 $\mathrm{kg\,m^{-3}}$	3,000 $\mathrm{kg\,m^{-3}}$
Young's modulus	30,000 MPa	3,000 MPa	7,500 MPa
Poisson's ratio	0.18	0.18	0.18

Table 5.2: Maximum stress results of the FEM analysis.

with internal pressure	
Max. shear stress [MPa]	0.224
Max. tensile stress [MPa]	0.349
Max. compressive stress [MPa]	0.104
without internal pressure	
Max. shear stress [MPa]	0.02
Max. tensile stress [MPa]	0.041
Max. compressive stress [MPa]	0.016

tensile stress is 0.041 MPa and the maximum compressive stress is 0.016 MPa. Shear and tensile maximum stress is located similar as for the case with internal pressure, whereas the maximum compressive stress is located at the top of the inner cylinder near the front face of the structure.

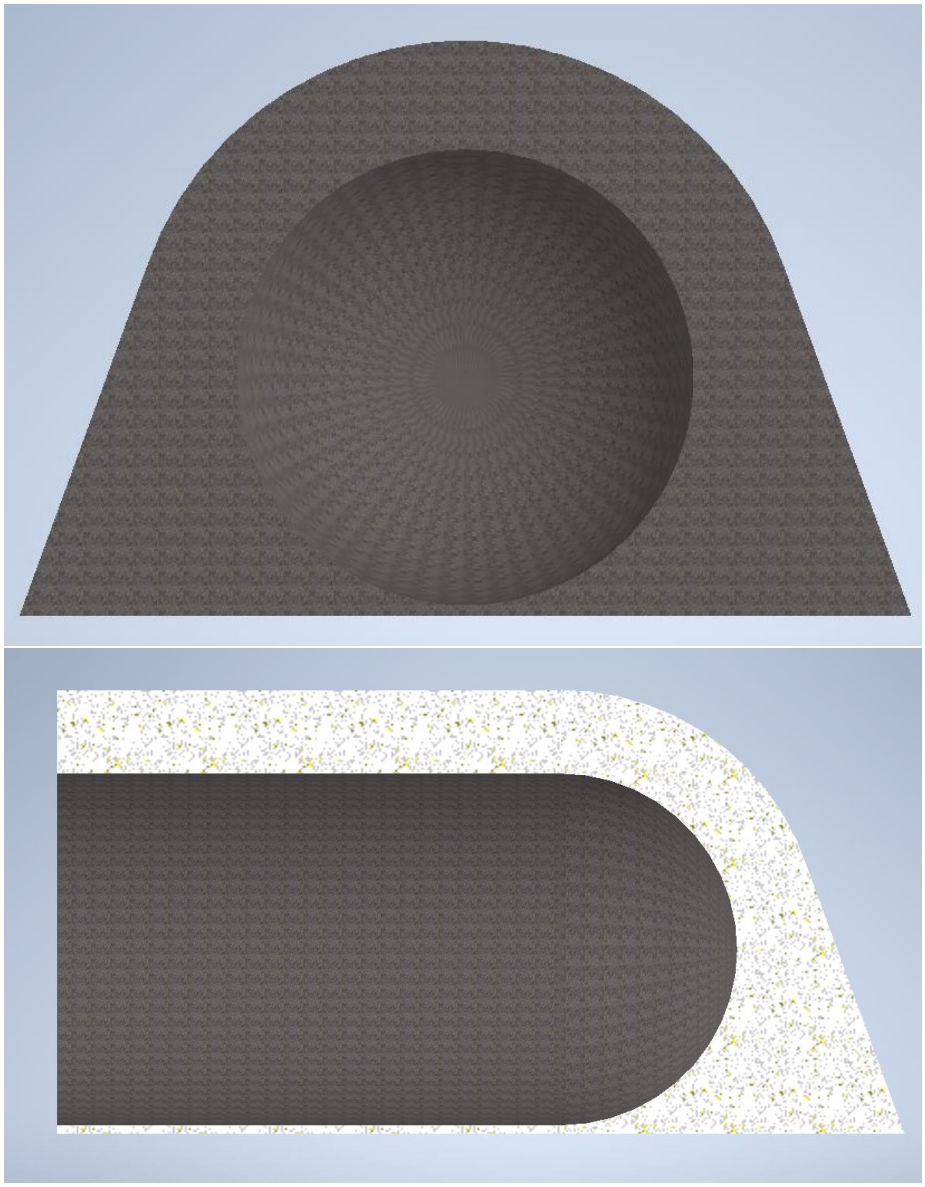

Figure 5.2: Regolith shielding manufactured with sintering. Top image is showing the front view and the lower image is showing the side view in half section.

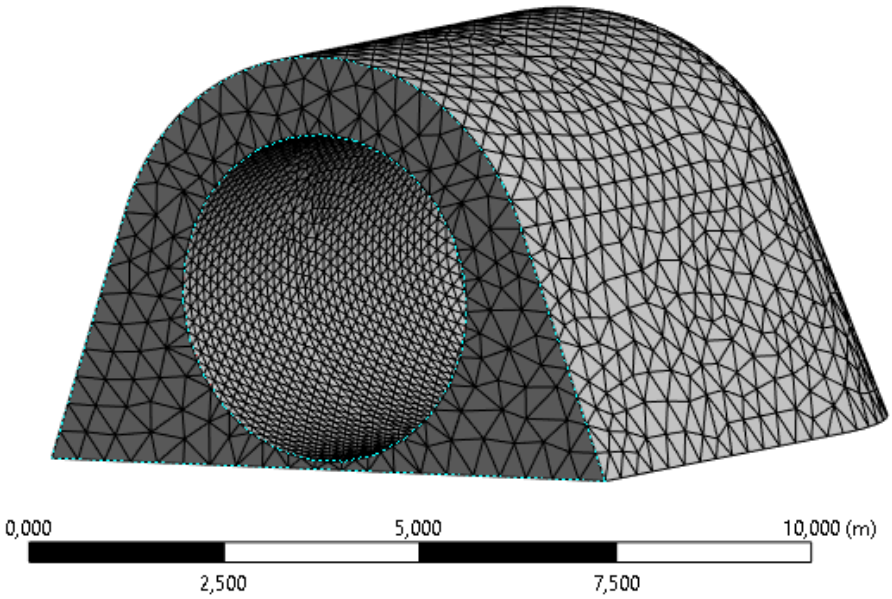

Figure 5.3: Meshed regolith structure with an element size of 0.4 m *and* 0.2 m *at the inner surface. Elements are created using the 'Body Sizing' method implemented in ANSYS. The elements are tetrahedral elements of second order.*

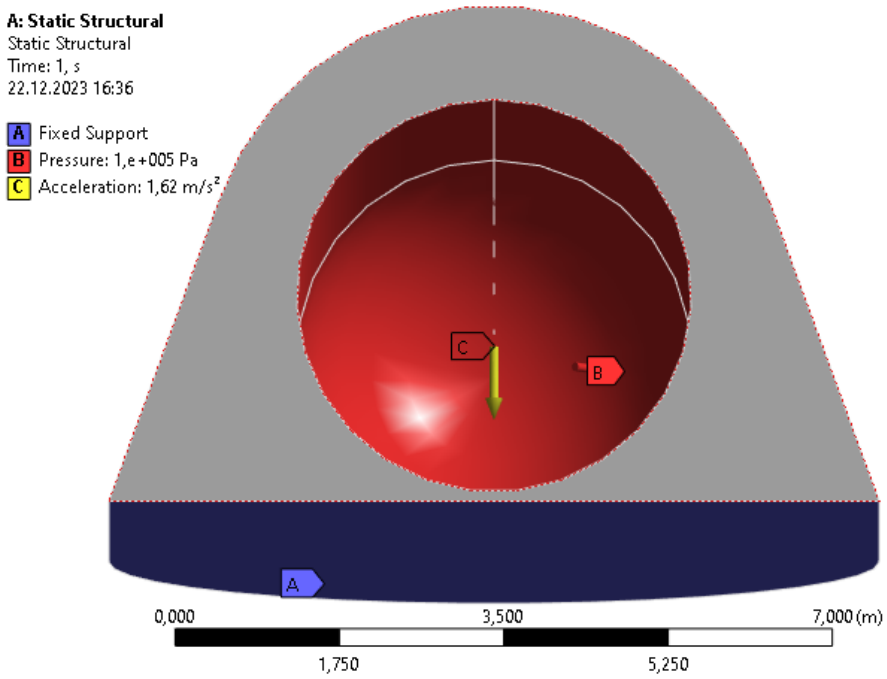

Figure 5.4: FEM setup. The model is fixed at the bottom and an acceleration of $1.62\ \mathrm{m\,s^{-2}}$ *simulates the lunar gravity. Optional an inner pressure of* 0.1 MPa *is acting at the inner surface to simulate the pressurized inflatable.*

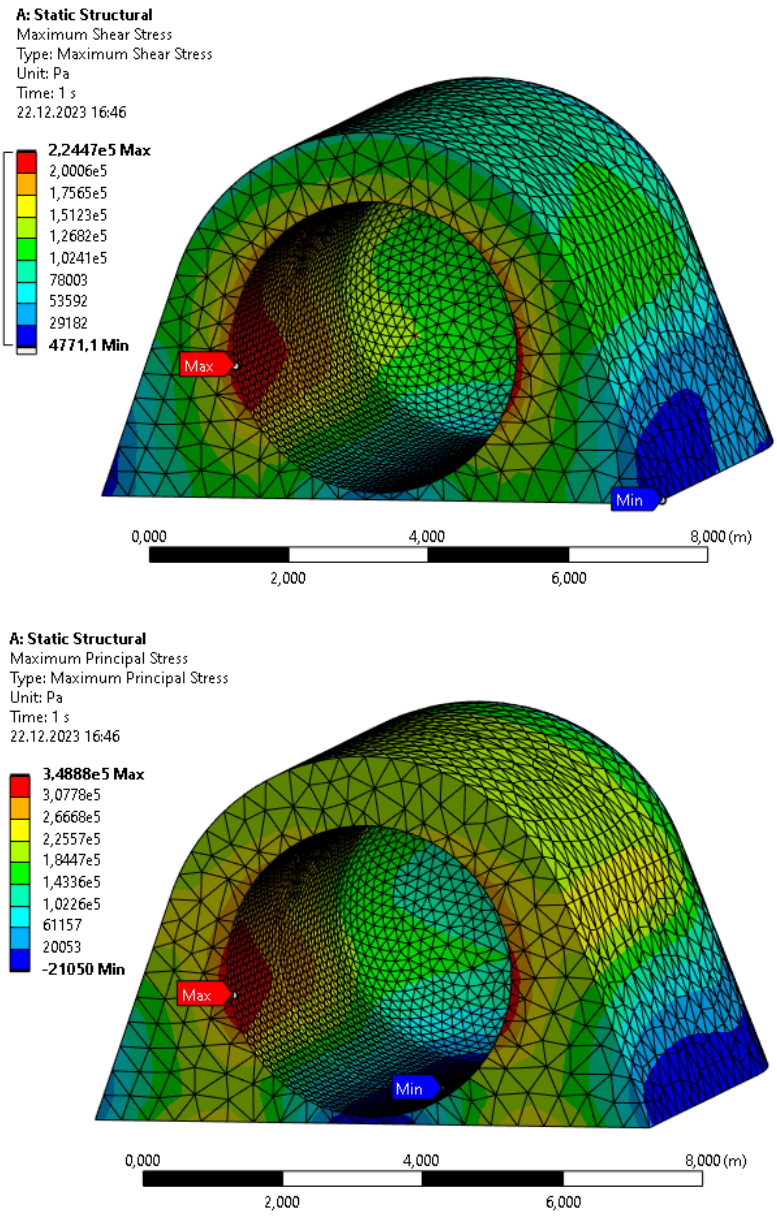

Figure 5.5: Stress results of the FEM analysis with internal pressure. The top images shows the shear stress and the bottom image shows the maximum principal stress. The positive values resemble the maximum tensile stress and the negative values resemble the minimum compressive stress. Maxima of the tensile and shear stress are located at the same region.

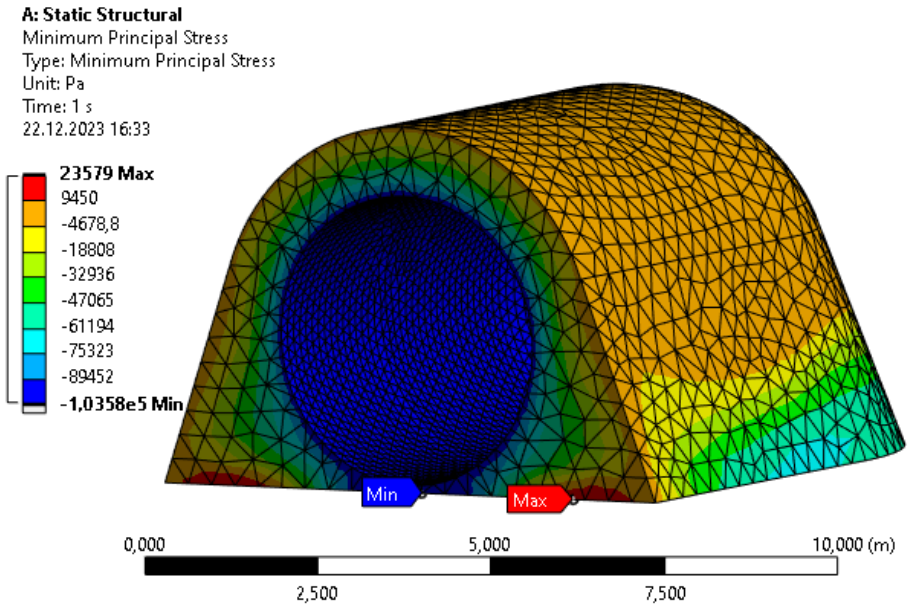

Figure 5.6: Minimum principal stress result of the FEM analysis with internal pressure. The negative values resemble the maximum compressive stress and the positive values resemble the minimum tensile stress. The maximum compressive stress sits at the inner surface and is slightly higher than the acting inner pressure.

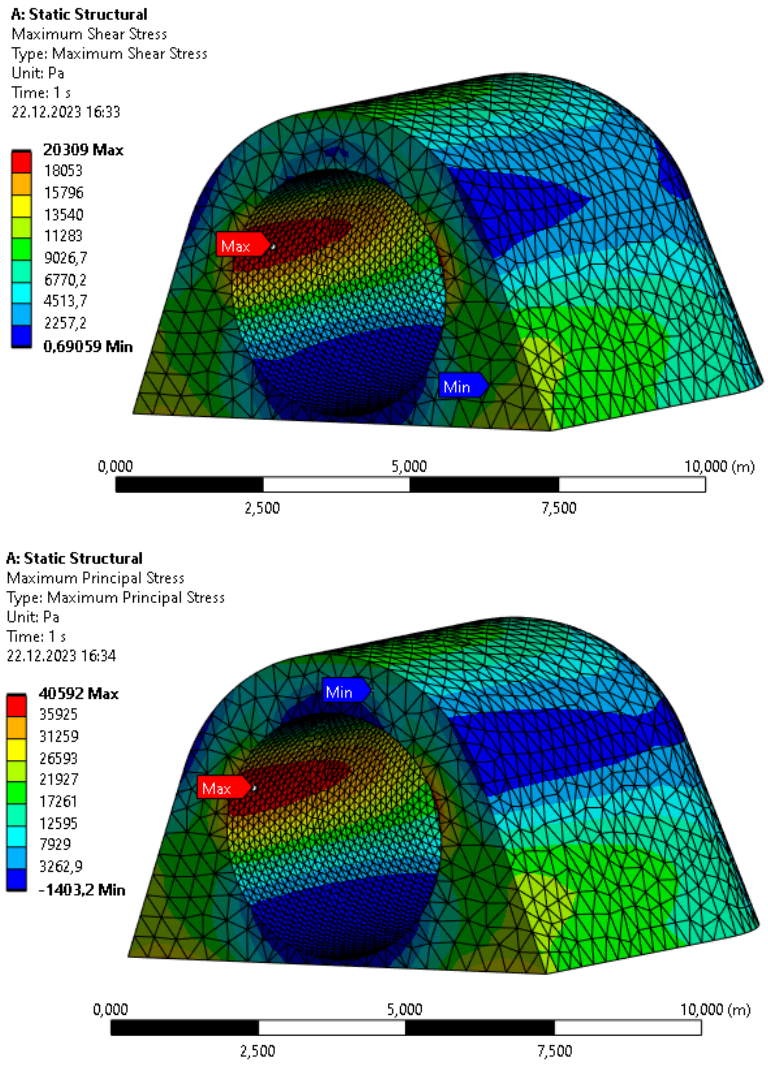

Figure 5.7: Stress results of the FEM analysis without internal pressure. The top images shows the shear stress and the bottom image shows the maximum principal stress. The positive values resemble the maximum tensile stress and the negative values resemble the minimum compressive stress. Maxima of the tensile and shear stress are located at the same region.

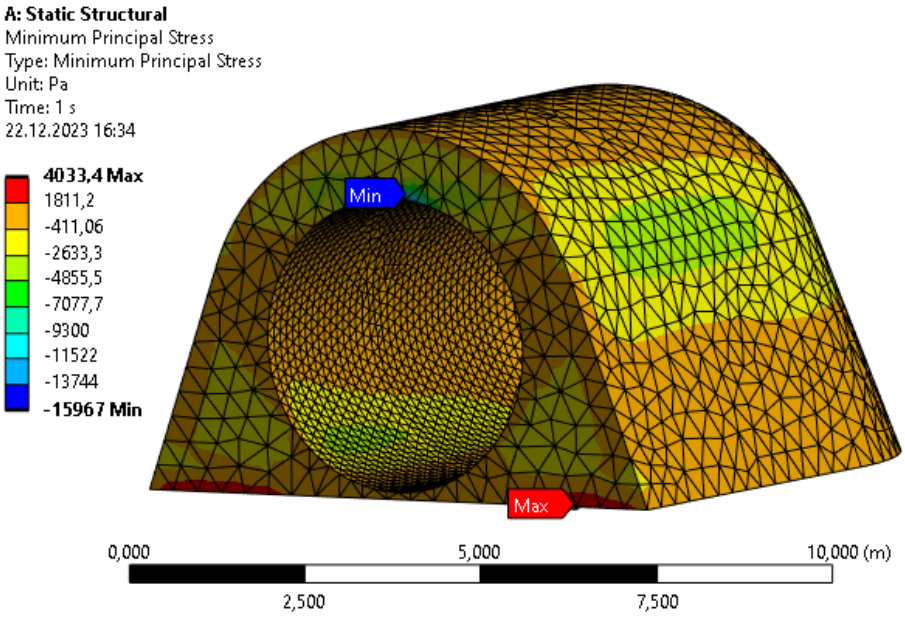

Figure 5.8: Minimum principal stress result of the FEM analysis without internal pressure. The negative values resemble the maximum compressive stress and the positive values resemble the minimum tensile stress. The maximum compressive stress sits at the face side right above the inner cylinder.

5.2.2 Secondary Structure

The interior desgin is divided into three different sections, the floor section including the floor structure and everything beneath, the growth area section and the ceiling section.

Floor Section

To have a plane ground surface in the cylindrical module, a floor needs to be installed. It will be composed of perforated panels similar to the EDEN NG design which are mounted on the supporting structure. One option for a supporting structure is shown in Figure 5.9. The beam is made out of aluminum, has a width of 10 cm and a mass of 36.52 kg. Potential necessary additional structure and interfacing elements are considered in the margin. Another option could be to choose a I-profile beam. With a panel size of 60 cm x 60 cm [70], 11 support elements are required which adds up to 482.08 kg for the support structure with a 20% margin . The weight of the panels is considered in the secondary structure mass of the EDEN NG design.

Growth Area Section

The growth area section will be similar to the design of EDEN NG with the International Standard Payload Racks (ISPR) as the main structural component. For mass assumptions the same mass for the EDEN NG is assumed for the growth area section. Only difference is that the ISPR's may need to be assembled inside the module due to their dimensions.

Ceiling Section

Main purpose of the ceiling section is to provide infrastructure such as piping and electronics, which can be mounted on top of the payload racks. Clamping

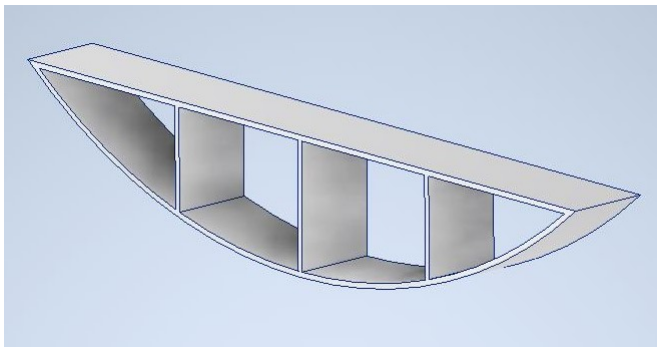

Figure 5.9: Potential design for a supporting structure element. It is separated in half for assembly.

or other holding mechanisms will not be described in detail, but are considered in the margin. Optional, panels can be installed between the ISPR's.

5.3 Discussion

5.3.1 Primary Structure

The regolith shielding of 1 m thickness made out of sintered regolith provides sufficient radiation shielding as the shielding of 300 g cm^{-2} leads to an effective dose equivalent (210 mSv/year) and BFO average dose equivalent (200 mSv/year) of $<$ 250 mSv/year [8].

FEM Discussion

Geometry

The maximum shear and tensile stress occur at the face of the structure. As the greenhouse module including the shielding will be connected to the habitat, it is expected that the maximum stresses at the face will be different. An additional analysis shall be performed once the habitat design is known.

Material Properties ('Engineering Data')

The physical material properties for the simulation were based on a given data set within the Ansys material library for concrete. Specific information on the concrete are not given and the potential impact on the properties can therefore not be investigated.
Additionally, scaling with respect to one specific property, in this case the compressive ultimate strength, was done because of lacking material data from literature. However, the proportional behavior was only assumed. Additional analysis with properties based on test data must be conducted.
Although the chemical composition of concrete and the sintered is quite similar, the binding mechanism can not be compared without further investigations. However, both material are brittle and are expected to have a compressive ultimate strength significantly larger than the tensile ultimate strength.

Homogeneous and isotropic material properties were assumed. More test data is necessary to evaluate this assumption. The layering of the material may have an impact here.

The density was defined as 3,000 kg m^{-3} according to the esa CFD study [8] but Khoshnevis et al. state a density of $>$ 1,900 kg m^{-3} [23]. 3,000 kg m^{-3} were used as a more conservative value to withstand the gravitation. Table 5.3 shows the maximum stress results with a lower density of 1,900 kg m^{-3} and the difference to the maximum stresses with the used density of 3,000 kg m^{-3} in percent (see Table 5.2). All maximum stresses are lower for the material with a lower density except for the compressive stress with internal pressure. However, the compressive stress increase of 1.83% is negligible for the factor of safety.

Table 5.3: Stress results using a density of 1,900 $\mathrm{kg\,m^{-3}}$*. They are compared with the stress results of Table 5.2 (density of 3,000* $\mathrm{kg\,m^{-3}}$*) and the stress delta is calculated.*

	Concrete with a Density of 1900 $\mathrm{kg\,m^{-3}}$	Stress Difference [%]
with internal pressure		
Max. shear stress [MPa]	0.22	-1.84
Max. tensile stress [MPa]	0.341	-2.22
Max. compressive stress [MPa]	0.104	0.18
without internal pressure		
Max. shear stress [MPa]	0.013	-37
Max. tensile stress [MPa]	0.026	-36.7
Max. compressive stress [MPa]	0.0026	-85

Setup

Pressure fluctuations of the inflatable are not considered in the simulation. They should not be critical due to the high safety factor against all three stresses.

Stresses introduced by temperature gradients and changes were not included. Additional thermal analysis is required. High thermal stresses could reduce safety factors.

Mesh

A mesh convergence and a nodes convergence analysis are performed to evaluate the mesh.
The mesh convergence analysis is done using the Richardson extrapolation and defining an error threshold of 1%. All investigated element sizes of 0.3 m - 0.6 m have an error of less than 1% except for the error of the compressive stress for an element size of 0.5 m (-1.8426%) (see Figure 5.10). The mesh used for the simulation (0.4 m and 0.2 m for the inner surface) has the lowest error for tensile (0.0574%) and shear stress (0.0268%). The errors are derived with respect to the stress value expected at an infinitesimal fine mesh.
Also the nodes are converging.
The used mesh is suitable for the simulation. A finer mesh is not required and limited because of the used product licence.

Results

Comparison of the simulated maximum shear, tensile and compressive stresses with the strength of the materials (see Table 5.1) indicates that the structure is stable for the investigated load cases even for the material with a compressive ultimate strength of 4 MPa as the safety factors listed in Table 5.4 are > 1.

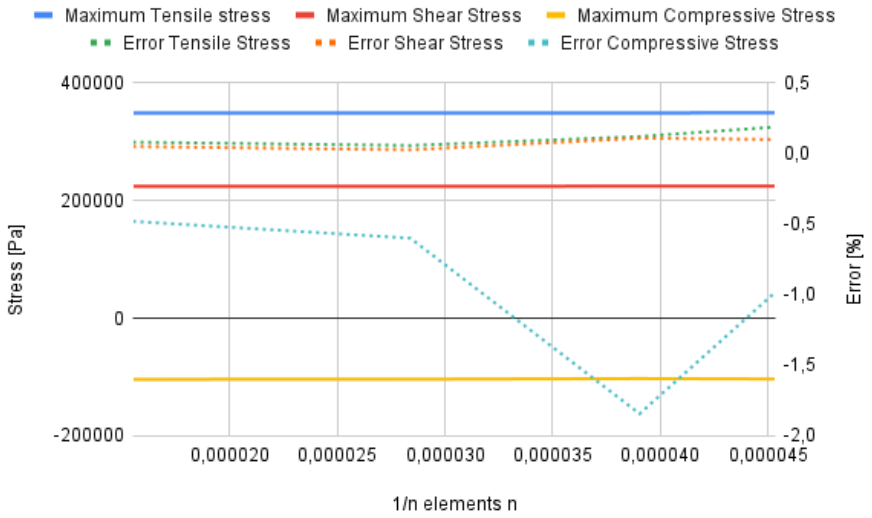

Figure 5.10: Mesh convergence using the Richardson extrapolation. The maximum tensile, shear and compressive stresses are over 1/n with n elements. The errors are derived with respect to the stress value expected at an infinitesimal fine mesh.

The factor of safety against shear stress is discussed in Chapter 5.3.2. There is no standard defining the factor of safety of sintered regolith structures yet. The ECSS-E-ST-32-10C standard defines for glass and ceramic structural parts an ultimate safety factor of 3.0 for human rated spacecrafts and the NASA JSC 65828 standard defines a safety factor of 2.0 for doors, hatches and habitat modules [71][72]. The ECSS-E-ST-32-10C standard states that there is no commonly agreed verification by analysis only for glass and ceramic structural parts in human rated spacecrafts [71]. Sintered regolith has a glassy phase and brittle properties which justifies the application of the factor of safety for glass and ceramic structural parts [26]. The more conservative factor of safety of 3.0 is used. Therefore, the scaled concrete with a compressive strength of 4 MPa does not have the required safety factor. The used material should provide a tensile strength of minimum 1.047 MPa, a compressive strength of minimum 0.311 MPa and a minimum shear strength of 0.674 MPa. For the concrete scaled with respect to the compressive strength this would be a compressive strength of 8.376 MPa. This also indicates that the compressive strength achieved with solar sintering by Meurisse et al. is not sufficient [26]. The main impact on the stress is introduced by the internal pressure which leads to high tensile stresses in the structure (see Table 5.2) which should be taken by the inflatable for the final design (see Chapter 5.3.3). This already indicates what shear and tensile stresses the inflatable must be capable to take (see Table 5.2). The simulated

Table 5.4: Safety factors of the concrete from the ANSYS libratory (LIB.) and both scaled concretes. Maximum stress results from Table 5.2 are compared with the material properties listed in Table 5.1. The factor of safety against shear stress is discussed in Cahpter 5.3.2.

Concrete Type (Compressive Strength)	Safety Factor Tensile Stress	Safety Factor Shear Stress	Safety Factor Compressive Stress
without internal pressure			
Ansys Lib. (40 MPa)	14.3	TBD	386.2
Scaled (4 MPa)	1.4	TBD	38.6
Scaled (10 MPa)	3.6	TBD	96.5
with internal pressure			
Ansys Lib. (40 MPa)	123.2	TBD	2505.6
Scaled (4 MPa)	12.3	TBD	250.6
Scaled (10 MPa)	30.79	TBD	626.4

compressive stresses at the inner surface of max 0.104 MPa are similar to the internal pressure of 0.1 MPa.

As the greenhouse module will be docked onto the habitat and the regolith shieldings connected as well, the stress near the face side differ from the real case. This has not been considered in the analysis as the habitat design is not fixed yet. Simulating the habitat interface with a fixed support at the face side reduces the maximum stresses. However, new and higher local maxima are introduced which are caused by the set up of the simulation. For shear and tensile stress they are located at the rim of the inner cylinder and for the compressive stress it is at the upper rim at the face side of the regolith structure (see Figure 5.11 and 5.12). The simulation set up fails here to resemble the real structure. This shows that the connection of the habitat shielding with the greenhouse shielding has a major impact on the maximum stress results of the greenhouse shielding.

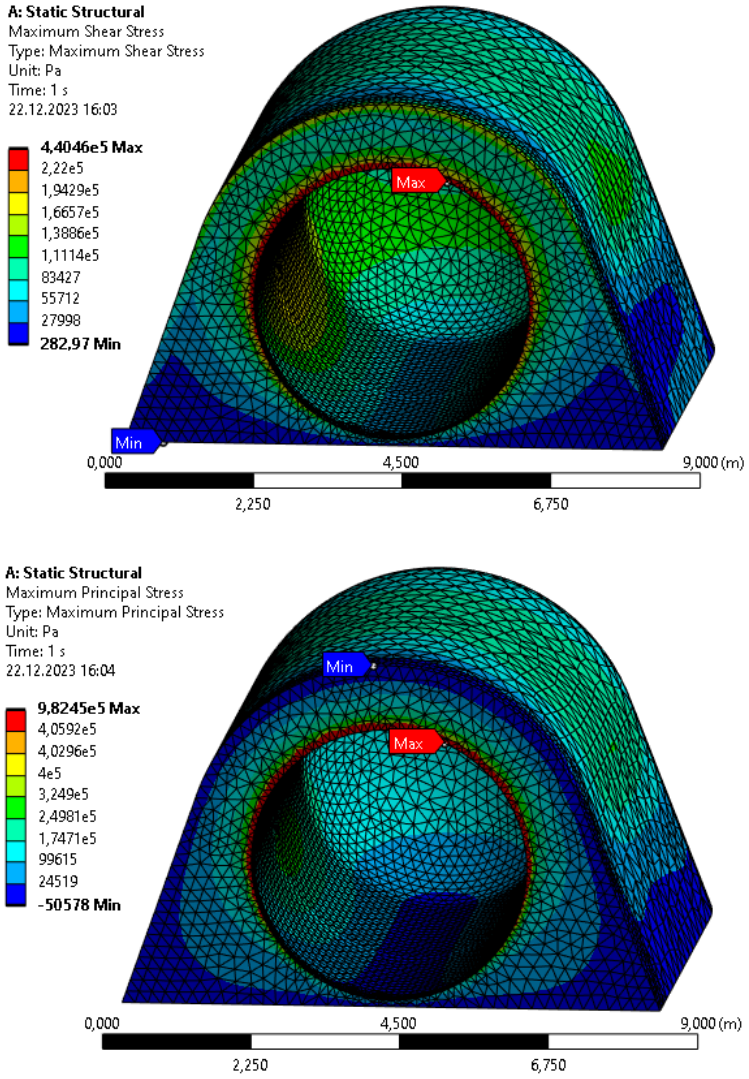

Figure 5.11: Stress results with an additional fixed support at the face side to simulate a connection to the habitat. The top image shows the maximum shear stress and the bottom image shows the maximum principle stress with the positive values resembling the tensile stress. Dark red indicates the locations with a maximum larger than simulated in Figure 5.5. Maxima are located for both at the rim of the inner surface which indicates a problem with the simulation setup. Prior local maxima (see Figure 5.5) are reduced indicating that the connection to the habitat impacts the stress results.

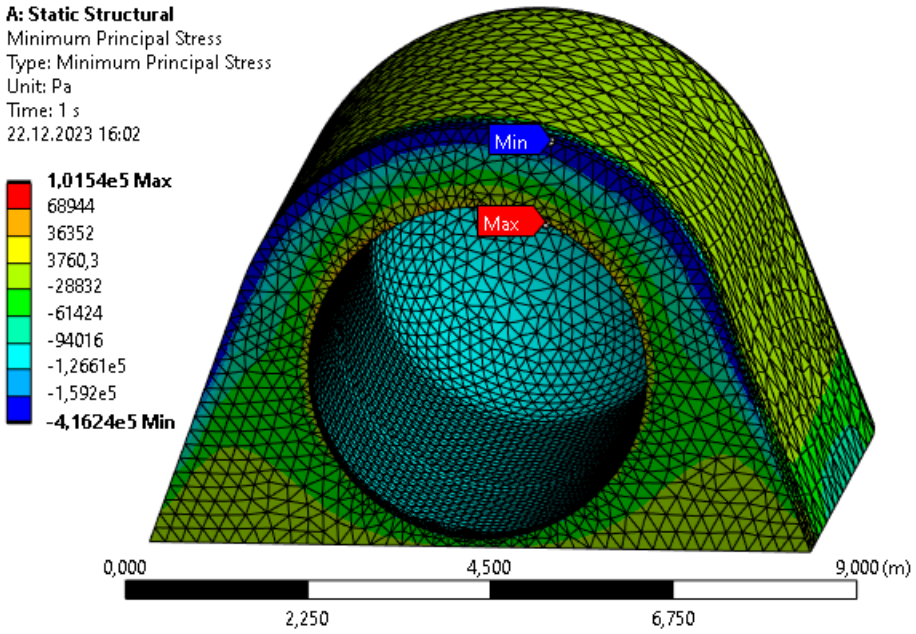

Figure 5.12: Minimum principle stress results with an additional fixed support at the face side to simulate a connection to the habitat. Negative values resemble the compressive stress. Dark blue indicates the locations with a maximum larger than simulated in Figure 5.6. The maximum is located at the upper rim of the structure at the face side which indicates a problem with the simulation setup. Prior local maxima (see Figure 5.6) are reduced indicating that the connection to the habitat impacts the stress results.

5.3.2 Open Issues

The shear strength of concrete depends on the geometry of the structure. For a beam element the nominal shear strength V_n is calculated according to Equation 5.1 with the compressive strength f_c, the depth of the beam h, the width of the beam b_w and the modification factor λ [73]. The regolith structure is more complex and the shear strength will differ in the structure.

$$V_n = \frac{4}{3}\lambda\sqrt{f_c}b_w h[73] \tag{5.1}$$

The shear strength has not been analysed yet due to time restrictions. The structure has a minimum thickness of 1 m and cutting out one 1 m x 1 m element and assuming a modification factor of 1 for normal weight concrete and a compressive strength of 8.376 MPa would lead to a nominal shear strength of 3.859 MPa for this element which would be a sufficient safety factor > 3. However, a detailed analysis is necessary.

5.3.3 Outlook - Design

The adapter ring of the inflatable should be designed in further detail. Within this process the clamping mechanism should be investigated and tested. A smaller scaled model may be created for test purposes.

An additional analysis should include the inflatable as it is expected that the more stiff inflatable takes a significant part of the shear and tensile stresses. The regolith structure should be further optimized. Due to the higher compressive strength of the material, the structure should be designed such that most stresses are compressive. Additional analysis should include a thermal analysis and use material data obtained from test campaigns to prevent errors caused by scaling.
As mentioned in Chapter 5.3.2 a shear strength analysis of the structure shall be performed in future work.

Also the secondary structure should be designed in more detail. Especially the interface to the inflatable needs careful investigation as it is the main difference of the secondary structure compared with the EDEN NG design.

Chapter 6

Mission

This chapter combines the previous results to design the mission. The mission process is described, the mass budget listed and a cost-benefit analysis compares the elaborated mission concept with the EDEN NG concept.

6.1 Method

The mission is defined and described based on the results of Chapter 4 and 5. A cost/benefit analysis is performed. The transport mass is the only considered parameter. Other costs such as development costs are complex to estimate at this stage and therefore not part of this thesis. Transport costs, especially to the lunar surface, are a big fraction of the total mission costs. Astrobotics for example prices one kilogram payload to the lunar surface with 1.2 million $ [74]. The costs per kilogram are similar for the Peregrine and the Griffon lander although the payload capacities are different by the factor 5 [74].

6.2 Results

6.2.1 Mission Process

Figure 6.1 shows a block diagram of the mission process. The process starts with the cargo delivery at the lunar surface. With the mobile crane available (See Chapter 4.1), the components are unloaded and transported to respective sites. All equipment is then prepared for further work. It is unpacked, checked and if necessary batteries are charged. Once the functionality is given, the process starts with the excavation of the first regolith batches. At the construction site a foundation is sintered to provide better stability and a plane surface. After this step the inflatable is connected to the habitat while still being in a folded transport configuration to protect it against impact of micro meteoroids and damages during construction. Once the regolith structure is finished, the inflatable can be pressurized into the mold of the regolith structure. Then

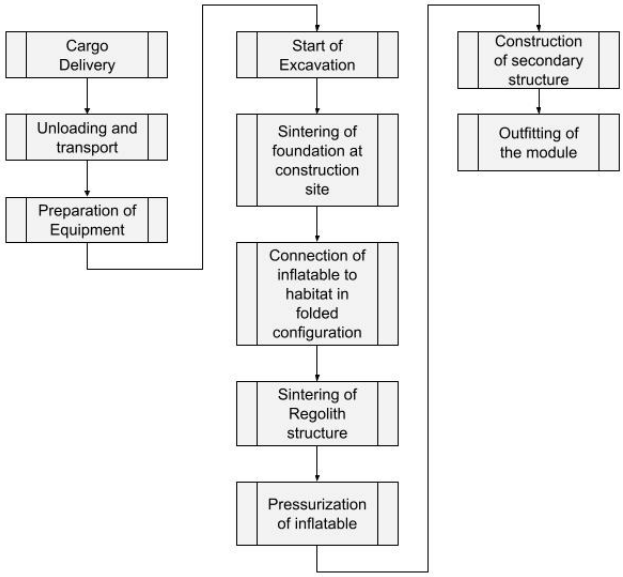

Figure 6.1: Block diagram of the mission process to manufacture a greenhouse module on site. The mission starts with the cargo delivery and the unloading of the equipment and the transport to the respective sites. The equipment is then prepared which includes functionality tests. The manufacturing process begins with the start of the excavation. The foundation is sintered first. After that, the folded inflatable is connected to the habitat. It stays folded until the regolith shielding is finalized to prevent damages during construction. Once the inflatable is pressurized the secondary structure can be constructed in the inflatable. The mission is finished with the outfittng of the greenhouse module.

finally the secondary structure, so the floor, growth area and ceiling can be build together inside the greenhouse module and outfitted with the rest of the equipment. Figure 6.2 shows a rendering of the greenhouse module on the lunar surface.

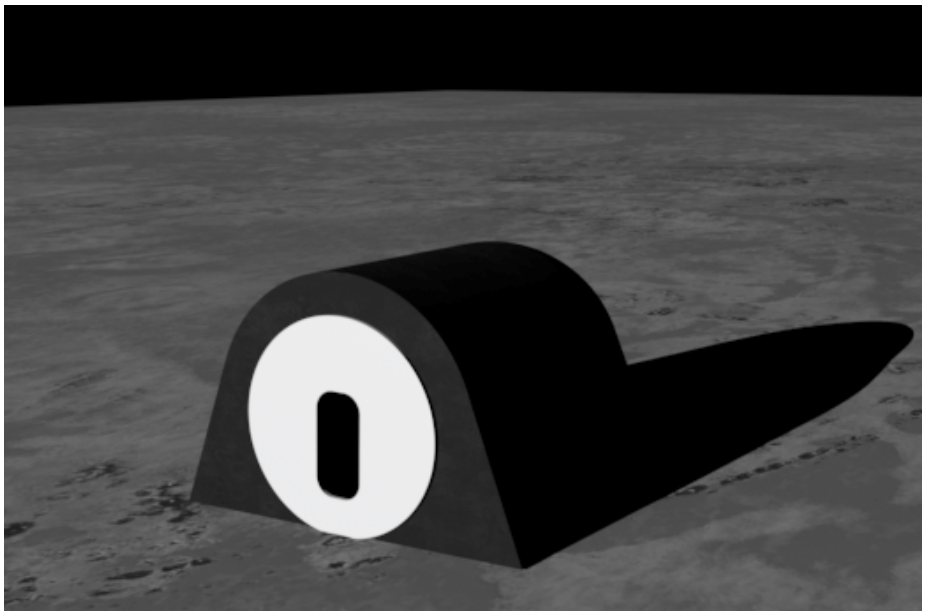

Figure 6.2: Rendering of the greenhouse module on the lunar surface. It includes the inflatable and the regolith structure.

6.2.2 Mass Budget Overview

The mass of the mission concept is mainly composed of the manufacturing method, the inflatable, the secondary structure and others such as secondary payload (Crops).
Table 6.1 shows an overview of the mass budget of the mission using the laser sintering method (see Chapter 4.3.2). The mass for all manufacturing methods is shown in Tables 4.1-4.7. The inflatable mass is estimated in Chapter 5.2.1. The secondary structure mass is composed of the support structure elements described in Chapter 5.2.2 and the secondary structure mass described by Schubert et al. of 517.275 kg including a 10% margin for necessary modifications [7]. The rest is based on the EDEN NG design and adds up to 3,889.79 kg.

6.2.3 Cost-Benefit Analysis

The transport mass will be the main investigated parameter for the cost-benefit analysis as mentioned in Chapter 4.1.
Table 6.1 shows that it is estimated to transport 12,950 kg to the lunar surface to build the first greenhouse module with laser sintering and an inflatable.
The cargo-to-green approach on the other side adds up to 11,763 kg (see Chapter 1.2). However, this number does not include the regolith shielding as it is assumed that the already existing method is used.

Table 6.1: Mass budget overview of the mission.

Subsystem	Mass [kg]
Manufacturing Process (Laser Sintering)	2,200
Secondary Structure	999.35
Inflatable	5,860.5
Rest	3,889.8
Total	12,950

The transport mass for the manufacturing method are only one time transport costs. Once the infrastructure is brought to the lunar surface for the first module, each module requires 10,749.6 kg transport mass which is 1,013.4 kg less than the cargo-to-green approach.

6.3 Discussion

6.3.1 Cost-Benefit Analysis

Two greenhouse modules of the manufacturing on-site approach costs 23,196.21 kg transport mass whereas the EDEN NG approach costs 23,526 kg. From a transport mass perspective, the approach to manufacture the greenhouse module on site is cheaper if more than one module is planned.
If it is assumed, like for the EDEN NG project, that the infrastructure for the regolith shielding is already on site available, the suggested approach is cheaper right from the start. Astrobotic's prices the transport costs to the lunar surface with 1.2 million $ for their Griffin Lander that has a payload capacity of 600 kg [74]. So, the transport costs of the first greenhouse module using the elaborated manufacturing method would cost 15.4 billion $ and every additional module would cost 13.9 billion $. The mass savings compared to the EDEN NG approach could save 1.2 billion $. Even if costs decrease significantly, it will be still profitable to use the approach elaborated in this work.

6.3.2 Outlook - Mission

The cost-benefit analysis should be expanded with more parameter than the estimated mass. Parameters of interest include volume, power and crew time. All can be compared calculating the equivalent system mass. Another point to consider are the development costs.

Chapter 7

Overarching Discussion

7.1 Justification against Requirements

Table 7.1 justifies the design and manufacturing process against the requirements defined in Table 3.1. Most requirements are met. However, a thermal analysis and an investigation of the time parameter shall be performed.

87

Table 7.1: Justification of the mission conept against the defined requirements. Except for SYS-07 all requirements are met.

SET-01	The time parameter has not been investigated.
SET-02	The environment near the Shackelton crater rim at the southpole has been considered.
SET-03	N/A
SET-04	N/A
SET-05	The power consumption of the manufacturing methods was considered in the trade-off.
SYS-01	The regolith structure is completely manufactured with on site materials. Due to little knowledge on air tight regolith structures, an inflatable with an adapter ring needs to be transported for every new module.
SYS-02	The volume of the inflatable can be pressurized.
SYS-03	The pressurizable volume is 102.52 m^3.
SYS-04	The connection to the habitat was considered by including an adapterring. The detailed conection interface is not designed until the habitat interface is known.
SYS-05	The system is capable to shield the crew against radiation (see Chapter 5.3.1).
SYS-06	According to Ceccanti et al., the regolith shielding of 1 m with a density of 3,000 $kg\,m^{-3}$ is sufficient [6].
SYS-07	A thermal investigation has not been performed.

7.2 Missing Considerations

One parameter that was not considered yet in this thesis and in the trade-off is the psychological factor.
Far away from the home planet in a harsh and deadly environment a secure habitat is desired by the astronauts. Non rigid structures may meet this desire from a technological perspective, but this may be different from a psychological perspective. As no research on this topic was found, it was excluded for this thesis but should be mentioned. However, the greenhouse module will not be the complete habitat and other retreats are possible. It is also possible that the secondary structure and the plants cover most of the inflatable.

Also not investigated was the time parameter. The construction time including the regolith processing was not considered in the trade-off. This was done because of lacking data. Especially the research around the regolith processing is lacking information about duration's.

The time parameter was only considered for the excavation as the regolith processing was scaled with respect to the excavation rate and too low excavation

rates could potentially lead to too low and unrealistic transport masses. The choice to use ten excavators was made as roughly one month was assumed as a more reasonable time than roughly ten month. For the laser sintering method this led to a mass increase of 36% for the manufacturing method and of 5.5% for the first greenhouse module. Time constraints for a mission has a direct impact on the mission costs.

Although reinforcement is mentioned in the state of the art, it is not further considered for the design. Using additives in the concrete mixture could improve radiation shielding or other material properties such as tensile strength. The elaborated design does not include or build on these potential improvements. However, they should be considered if the concept reaches a higher maturity.

7.3 Outlook

The outlook regarding the manufacturing method, the design and the mission are discussed in the Chapters 4.3.5, 5.3.3 and 6.3.2.

Chapter 8

Conclusion

The return of humanity to the Moon will include long term presence of humans on the lunar surface. The greenhouse module EDEN from DLR is planned to be added to a potential lunar habitat to provide fresh food that is difficult to transport, decrease the food transport and dependency in the long term, increase the well being factor and work as a biogenerative life support system. The current approach of the EDEN NG project is a cargo-to-green approach in which the module is utilized as a cargo during transfer and then as a greenhouse module. Purpose of this thesis was to analyse and evaluate an in-situ resource utilization based structure of the lunar greenhouse.

After a literature research, six different manufacturing methods were elaborated and evaluated in a trade-off. One manufacturing method was defined which is the most suitable to manufacture one part of the primary structure of the green house module with resources available on site. The best performing manufacturing method are the solar and laser sintering methods with the laser sintering method performing slightly better. With adapted weighting, which has a focus on the complexity of the manufacturing method, the complexity of the regolith processing and the required mass, both are performing similar. Further investigation including a more advanced system design and test data is necessary to make a final decision between solar and laser sintering. The principle is similar for both. An energy beam sinters the layered and sieved regolith to create a solid stucture. Only the energy beam is different. For solar sintering, the beam is concentrated solar light and for laser sintering it is created by ten CO_2 lasers.

Based on the chosen manufacturing method, the primary structure was designed. It is composed of an inflatable including an adapter ring to dock onto the habitat and the sintered regolith shielding. The regolith shielding was analysed using FEM. The results indicate that the design is stable if the material has a tensile strength of minimum 1.047 MPa, a compressive strength of minimum 0.311 MPa and a minimum shear strength of 0.674 MPa which includes a safety factor of 3.0.

The secondary structure is composed of the floor section, which is mounted onto custom designed profiles, the growth area, which is based on international standard payload racks and the ceiling section which houses the required piping and cabling.

Once the components are unloaded from the lander and transported to the habitat site, components are tested and the manufacturing process is started. The components for the manufacturing process have a mass of 2,200 kg. The inflatable with a weight of 5,860.5 kg is docked onto the habitat with no internal pressure to prevent damages during construction. After finished manufacturing of the regolith structure, the inflatable is pressurized. The secondary structure with a total mass of 5,860.5 kg is then installed inside the inflatable. Components may need to be build together inside the inflatable. The rest of the equipment (3,889.8 kg) which is similar to the EDEN NG approach is then installed. The first greenhouse module requires the transport of 12,950 kg to the lunar surface. Depending on development of transport costs to the lunar savings, the transport costs could be decreased by 1.2 billion $ compared to the EDEN NG approach.

This work indicates that it is possible to manufacture in-situ resource utilization based structures of a lunar greenhouse using a laser sintering method. It is currently not possible to manufacture pressurizable structures with regolith only. Inflatables should be used to keep the pressure in the module. From a transport mass perspective this approach is cheaper than the cargo-to-green approach if more than one module is built. If the necessary infrastructure for regolith structure manufacturing is available on site, the elaborated method is cheaper from the first module on.

Future research should elaborate the laser and solar sintering process in more detail until building a prototype of the rover. The design should be optimized and analysed also for the temperature. The time paramter should be investigated in future research.

Bibliography

[1] National Aeronautics and Space Administration NASA. "NASA's Lunar Exploration Program Overview". In: (Sept. 2020). NP-2020-05-2853-HQ.

[2] Kathryn Hambleton. *NASA's First Flight With Crew Important Step on Long-term Return to the Moon, Missions to Mars*. 2018. URL: https://www.nasa.gov/feature/nasa-s-first-flight-with-crew-important-step-on-long-term-return-to-the-moon-missions-to (visited on 08/09/2023).

[3] mdr (kie). *SpaceX will bis 2029 Menschen auf den Mars bringen*. 2022. URL: https://www.mdr.de/wissen/spacex-diese-dekade-menschen-auf-den-mars-starship-musk-shotwell-100.html (visited on 08/09/2023).

[4] SpaceX. *Starship*. URL: https://www.spacex.com/vehicles/starship/ (visited on 01/09/2024).

[5] Christiane Heinicke and Cyprien Verseux. "The MaMBA facility as a testbed for bioregenerative life support systems". In: *Life Sciences in Space Research* 36 (2023), pp. 86–89. ISSN: 2214-5524. DOI: https://doi.org/10.1016/j.lssr.2022.08.009. URL: https://www.sciencedirect.com/science/article/pii/S2214552422000669.

[6] F. Ceccanti et al. "3D printing tecnology for a moon outpost exploiting lunar soil". In: 61th International Astronautical Congress IAC 2010. Sept. 2009.

[7] Volker Maiwald et al. "From Antarctic prototype to ground test demonstrator for a lunar greenhouse". In: *Acta Astronautica* 212 (2023), pp. 246–260. ISSN: 0094-5765. DOI: https://doi.org/10.1016/j.actaastro.2023.08.012. URL: https://www.sciencedirect.com/science/article/pii/S0094576523004101.

[8] R. Biesbroek et al. *CDF Study Report Moon Village Conceptual Design of a Lunar Habitat*. CDF Study Report CDF-202(A). esa concurrent design facility, 2020.

[9] Grant Heiken, David Vaniman, and Bevan French. "Lunar sourcebook - A user's guide to the moon". In: (Feb. 1991).

[10] P. Carpenter et al. "Development of Standardized Lunar Regolith Simulant Materials". In: *Microscopy and Microanalysis* 12 (Aug. 2006), pp. 886–887. DOI: 10.1017/S143192760606301X.

[11] Brian M. Willman et al. "Properties of Lunar Soil Simulant JSC-1". In: *Journal of Aerospace Engineering* 8.2 (1995), pp. 77–87. DOI: 10.1061/(ASCE)0893-1321(1995)8:2(77).

[12] Gunter Just et al. "Parametric review of existing regolith excavation techniques for lunar In Situ Resource Utilisation (ISRU) and recommendations for future excavation experiments". In: *Planetary and Space Science* 180 (Sept. 2019), p. 104746. DOI: 10.1016/j.pss.2019.104746.

[13] Robert P. Mueller et al. "Design of an Excavation Robot: Regolith Advanced Surface Systems Operations Robot (RASSOR) 2.0". In: *Earth and Space 2016*, pp. 163–174. DOI: 10.1061/9780784479971.018.

[14] Robert Mueller et al. "Additive Construction with Mobile Emplacement (ACME)". In: (Sept. 2017). 68th International Astronautical Congress.

[15] Gunter Just et al. "Development and test of a Lunar Excavation and Size Separation System (LES 3) for the LUVMI-X rover platform". In: *Journal of Field Robotics* 39 (Nov. 2021), pp. 263–280. DOI: 10.1002/rob.22050.

[16] J.N. Rasera et al. "The beneficiation of lunar regolith for space resource utilisation: A review". In: *Planetary and Space Science* 186 (2020), p. 104879. ISSN: 0032-0633. DOI: https://doi.org/10.1016/j.pss.2020.104879. URL: https://www.sciencedirect.com/science/article/pii/S0032063319301266.

[17] M. Adachi et al. "Particle-size sorting system of lunar regolith using electrostatic traveling wave". In: *Journal of Electrostatics* 89 (2017), pp. 69–76. ISSN: 0304-3886. DOI: https://doi.org/10.1016/j.elstat.2017.08.002. URL: https://www.sciencedirect.com/science/article/pii/S0304388617300153.

[18] Eric L. Christiansen, Charles H. Simonds, and K. O. Fairchild. "Conceptual Design of a Lunar Oxygen Pilot Plant". In: (1988). URL: https://api.semanticscholar.org/CorpusID:109694532.

[19] Hong Jiao, Chang Shi, and Rui Tian. "Research on Design and Magnet Assembly Process of Multivariate and Multi-Roll Permanent Magnetic Separator". In: *Advanced Materials Research* 201-203 (Feb. 2011), pp. 486–490. DOI: 10.4028/www.scientific.net/AMR.201-203.486.

[20] Francisco Javier Guerrero Gonzalez. "Analysis of an In-Situ Material Production Concept for Potential Thermal Applications in a Lunar Mission". MA thesis. Chair of Astronautics, Technical University of Munich, 2022.

[21] Everett Gibson and G. Moore. "Sulfur abundances and distributions in the Valley of Taurus-Littrow". In: (Feb. 1974). Lunar Science Conference 1974.

[22] Ahmed Ibrahim. "Performance Assessment of a Sulphur Recovery Unit". In: (Feb. 2021). DOI: 10.23880/ppej-16000254.

[23] Behrokh Khoshnevis, Anders Carlson, and Madhu Thangavelu. *ISRU-Based Robotic Construction Technologies for Lunar and Martian Infrastructure NIAC Phase II Final Report*. HQ-E-DAA-TN41353. Dec. 2020.

[24] Shuai Li et al. "Direct evidence of surface exposed water ice in the lunar polar regions". In: *Proceedings of the National Academy of Sciences* 115 (Aug. 2018), p. 201802345. DOI: 10.1073/pnas.1802345115.

[25] Luca Kiewiet et al. "Trade-off and optimization for a thermal lunar water extractor". In: (Sept. 2022). IAC 2022.

[26] "Solar 3D printing of lunar regolith". In: *Acta Astronautica* 152 (2018), pp. 800–810. ISSN: 0094-5765. DOI: https://doi.org/10.1016/j.actaastro.2018.06.063. URL: https://www.sciencedirect.com/science/article/pii/S0094576518303874.

[27] Behrokh Khoshnevis et al. "Lunar Contour Crafting: A Novel Technique for ISRU-Based Habitat Development". In: *43rd AIAA Aerospace Sciences Meeting and Exhibit - Meeting Papers* (Feb. 2005). DOI: 10.2514/6.2005-538.

[28] Neil Leach et al. "Robotic Construction by Contour Crafting: The Case of Lunar Construction". In: *International Journal of Architectural Computing* 10 (2012), pp. 423–438.

[29] Mohammad Khorramshahi and Ali Mokhtari. "Automatic Construction by Contour Crafting Technology". In: *Emerging Science Journal* 1 (July 2017), p. 28. DOI: 10.28991/esj-2017-01113.

[30] Behrokh Khoshnevis, Anders Carlson, and Madhu Thangavelu. *Contour Crafting Simulation Plan for Lunar Settlement Infrastructure Build-Up NIAC Phase-I Final Project Report*. Oct. 2012. DOI: 10.1061/9780784412190.155.

[31] Giovanni Cesaretti et al. "Building components for an outpost on the Lunar soil by means of a novel 3D printing technology". In: *Acta Astronautica* 93 (2014), pp. 430–450. ISSN: 0094-5765. DOI: https://doi.org/10.1016/j.actaastro.2013.07.034. URL: https://www.sciencedirect.com/science/article/pii/S0094576513002889.

[32] Kevin Farries, Phillip Visintin, and Scott Smith. *Direct laser sintering for lunar dust control: An experimental study of the effect of simulant mineralogy and process parameters on product strength and scalability*. Sept. 2022. DOI: 10.1016/j.conbuildmat.2022.129191.

[33] Diego Urbina et al. "Robotic prototypes for the solar sintering of regolith on the lunar surface developed within the Regolight project". In: (Nov. 2017). International Astronautical Congress 2017.

[34] Hatice Cullingford and M. Keller. "Lunar concrete for construction". In: (Feb. 1988).

[35] G. Habert. "1 - Environmental impact of Portland cement production". In: *Eco-Efficient Concrete*. Ed. by F. Pacheco-Torgal et al. Woodhead Publishing Series in Civil and Structural Engineering. Woodhead Publishing, 2013, pp. 3–25. ISBN: 978-0-85709-424-7. DOI: https://doi.org/10.1533/9780857098993.1.3. URL: https://www.sciencedirect.com/science/article/pii/B9780857094247500013.

[36] Sujeong Lee and Arie van Riessen. "A Review on Geopolymer Technology for Lunar Base Construction". In: *Materials* 15.13 (2022). ISSN: 1996-1944. DOI: 10.3390/ma15134516. URL: https://www.mdpi.com/1996-1944/15/13/4516.

[37] Houssam A. Toutanji, Steve Evans, and Richard N. Grugel. "Performance of lunar sulfur concrete in lunar environments". In: *Construction and Building Materials* 29 (2012), pp. 444–448. ISSN: 0950-0618. DOI: https://doi.org/10.1016/j.conbuildmat.2011.10.041. URL: https://www.sciencedirect.com/science/article/pii/S0950061811005903.

[38] Philipp Gläser et al. "Temperatures Near the Lunar Poles and Their Correlation With Hydrogen Predicted by LEND". In: *Journal of Geophysical Research: Planets* 126.9 (2021), e2020JE006598. DOI: https://doi.org/10.1029/2020JE006598. URL: https://agupubs.onlinelibrary.wiley.com/doi/abs/10.1029/2020JE006598.

[39] Richard Grugel and Houssam Toutanji. "Sulfur "concrete" for lunar applications – Sublimation concerns". In: *Advances in Space Research* 41 (Dec. 2008), pp. 103–112. DOI: 10.1016/j.asr.2007.08.018.

[40] Houssam Toutanji and Richard Grugel. "Mechanical Properties and Durability Performance of "Waterless Concrete"". In: Sept. 2008, pp. 1–8. ISBN: 978-0-7844-0988-6. DOI: 10.1061/40988(323)46.

[41] David Cadogan et al. "Intelligent Flexible Materials for Deployable Space Structures (InFlex)". In: (May 2006). DOI: 10.2514/6.2006-1897.

[42] Melanie Bodiford et al. "In situ resource-based lunar and martian habitat structures development at NASA/MSFC". In: *A Collection of Technical Papers - 1st Space Exploration Conference: Continuing the Voyage of Discovery* 2 (Feb. 2005). DOI: 10.2514/6.2005-2704.

[43] *Concurrent Design Facility Studies Standard Margin Philosophy Description*. Standard. European Space Agency, Aug. 2017.

[44] RUSSEL. *Russel Compact Sieve*. URL: https://www.russellfinex.com/en/separation-equipment/screening-machines/vibratory-sieves/ (visited on 12/13/2023).

[45] *Einbau- und Betriebsanleitung RUSSELL Compakt-Siebmaschinen*. CS/5 German. RUSSEL FINEX. Feb. 2009.

[46] Guillaume Habert. "Environmental impact of Portland cement production". In: Dec. 2013, pp. 3–25. ISBN: 9780857094247. DOI: 10.1533/9780857098993.1.3.

[47] *Induced Roll Magnetic Separator*. MT-DS-002. Rev. 3. Mineral Technologies - A downer Company.

[48] LIMING Heavy Industry Science and Technology. *MTW Series European Technology Trapezium Mill*. URL: https://www.limingco.com/products/MTW_Series_European_Technology_Trapezium_Mill.html (visited on 12/13/2023).

[49] *Laboratory Chamber and Tube Furnaces*. PL 1 / 05.09. THERMCONCEPT Dr. Fischer GmbH and Co. KG.

[50] *R88M-1@ 1S servo motor*. $\mathrm{SysCat}_I 189E - EN - 04C$. OMRON.

[51] Matthew Heverly et al. "Development of the TriATHLETE Lunar Vehicle Prototype". In: 2010. URL: https://api.semanticscholar.org/CorpusID:18788085.

[52] Matthew Heverly and Jaret Matthews. "A Wheel-on-limb rover for lunar operation". In: (Jan. 2008).

[53] *BLDC Motor Type BL80S*. no issue nr. accessed via https://www.powertronic.com/produkte/bldc-motoren/motoren-ohne-getriebe/bldc-bl80s/ at 10.01.2024. Powertronic.

[54] *Dobot CR Series User Guide*. Rev. V1.4. DOBOT. Oct. 2023.

[55] KITEC. *CTH500*. URL: https://kittec.eu/de/produkt/?ProduktID=CTH-500 (visited on 12/13/2023).

[56] *Water Cooled Shell and Tube Condensers*. DP-200-6 EN. BITZER.

[57] *2660 Series*. 850-4009. THOMAS by Gardener Denver. June 2017.

[58] Rabia, A. R., Ibrahim, A. H., and Zulkepli, N. N. "Activated alumina preparation and characterization: The review on recent advancement". In: *E3S Web Conf.* 34 (2018), p. 02049. DOI: 10.1051/e3sconf/20183402049. URL: https://doi.org/10.1051/e3sconf/20183402049.

[59] *CO2 and N2 Properties*. $0000082_0 718_T ICS$. LINDE Oil and Gas Services. July 2018.

[60] Vibra Schultheis. *Vibrationsmotoren HVL*. URL: https://www.vibra-schultheis.de/de/produkte/antreiben-aktivieren/kleinvibratoren-hvl-kv-ev.html (visited on 12/13/2023).

[61] DOBOT. *Mini Conveyor Belt Kit*. URL: https://www.dobot-robots.com/products/conveyor-belt/conveyor-belt-kit.html (visited on 12/13/2023).

[62] SINNTEC. *Ölpumpe - elektrisch - 1 l/min - 12V DC - Stahl (Artikelnummer 6303)*. URL: https://sinntec.de/Oelpumpe-elektrisch-1-l-min-12V-DC-Stahl (visited on 12/13/2023).

[63] *AQUASYSTEM® Replacable Membrane Potable Water Expansion Vessels*. POTVES-003-10/18. Reliance. Oct. 2018.

[64] *Diamond C-40 Series - Low Power CO^2 OEM Lasers for Marking and Engraving Applications*. https://sinntec.de/Oelpumpe-elektrisch-1-l-min-12V-DC-Stahl [Accessed: 13.12.2023]. COHERENT.

[65] dm folien. *KMF-Entsorgungssack 140 x 220 cm mit Bindeband*. URL: https://www.dm-folien.com/shop/kmf-entsorgungssack-140-x-220-cm-mit-bindeband (visited on 12/13/2023).

[66] KUKA. *KR 300-2 PA*. URL: https://www.kuka.com/de-de/produkte-leistungen/robotersysteme/industrieroboter/kr-300-pa (visited on 12/13/2023).

[67] Philipp Gläser et al. "Illumination conditions at the lunar south pole using high resolution Digital Terrain Models from LOLA". In: *Icarus* 243 (Aug. 2014), pp. 78–90. DOI: 10.1016/j.icarus.2014.08.013.

[68] Verya Ghasemipor and Saber Piroti. "Experimental Evaluation of the Effect of Water-Cement Ratio on Compressive, Abrasion Strength, Hydraulic Conductivity Coefficient and Porosity of Nano-Silica Concretes". In: *Journal of Applied Engineering Sciences* 8.2 (2018), pp. 17–24. DOI: doi:10.2478/jaes-2018-0013. URL: https://doi.org/10.2478/jaes-2018-0013.

[69] Ali Unal. "Production of metal powders by gas atomization". In: *Ulusal Toz Metalurjisi Konferansi: National Powder Metallurgy Conference* (Jan. 1996), pp. 111–157.

[70] *Raised floor Type VENTEC*. Rev. 02. LINDNER. Dec. 2017.

[71] *Structural factors of safety for spaceflight hardware*. Standard. European Cooperation for Space Standardization, Mar. 2009.

[72] *Structural Design Requirements and Factors Of Safety for Spaceflight Hardware*. Standard. This document represents the technical consensus of the developing group but does not yet have final NASA approval. National Aeronautics and Space Administration, July 2014.

[73] *Building Code Requirements for Structural Concrete*. Standard. American Concrete Institute, Sept. 2014.

[74] Astrobotic. *Landers*. URL: https://www.astrobotic.com/lunar-delivery/landers/ (visited on 12/13/2023).